Engineering and Technology Journal e-ISSN: 2456-3358

Volume 08 Issue 11 November -2023, Page No. - 3061-3083

DOI: 10.47191/etj/v8i11.16, I.F. – 7.136

Optimization of Thermo-Flow in a Solar Food Dehydrator Using Computational Techniques

K.E. Akpan[1], A. A. Okon[2], W.A. Akpan[3], I.I.Nyaudo[4]

[1, 2, 3] Department of Mechanical and Aerospace Engineering, University of Uyo, Nigeria

[4]Department of Mechanical Engineering, Federal University of Technology Ikot Abasi , Nigeria.

ABSTRACT: A solar food dehydrator converts solar energy into heat required to remove moisture from food. This study involved development of an optimized design for a solar dehydrator using computational techniques. A computer-aided design of six (6) different configurations of the dehydrator was developed, and a remotely-installed heat capture device was modelled and analysed using MATLAB. The results show that the Parabolic Trough Collector (PTC) could be used in effectively transferring heat remotely to a dehydrator. The temperature of air leaving the heat exchanger increases in proportion to the increase in the temperature of the heating fluid entering the heat exchanger. Computational Fluid Dynamics (CFD) in Ansys Fluent was employed to aid in the study of airflow and temperature distribution. The hot air was simulated at 2 m/s and 350 K inlet conditions. The CFD simulation results showed significant variations in the air velocity distribution and temperature for different configurations of the dehydrator. The back inflow - front outflow configuration provided the most uniform distribution of heated air in the drying chamber, with minimal variation on each tray. This uniformity was also observed in the distribution of static temperature. The back inflow – side outflow configuration showed a similar performance in flow and temperature distribution. However, the bottom inflow – top outflow and bottom inflow – front outflow configurations showed uneven velocity and temperature distribution inside the drying chamber. Supply of airflow across the trays horizontally provides best airflow and temperature distribution in solar dehydrators and thus highly recommended.

KEYWORDS: Thermo-flow, solar, energy, food, dehydrator, computational technique, optimization

1.0 INTRODUCTION

Heat is a measure of the temperature of a body. The scientific study of heat and degree of hotness of a body, its response to heat as well as how it can be used to operate or control other processes is known as thermodynamics [1].Eons of years ago, mankind has utilized heat energy in various forms for useful activities. Such activities include drying. [2] define drying as a process of reducing the moisture content of a material. It causes a decrease in chemical activity in the material; with a decrease in material mass and volume. Drying is a cost-effective method of food preservation. Dehydrated foods have longer shelf life [3],[4**]**. Typically, the sources of heat for drying include: electricity, infrared lamps, oil burners and solar power [2**]**

A dehydrator is a device which is designed to remove water from food materials by the application of heated air. Food dehydration depends on several factors including: product thickness, porosity, drying duration, temperature, operating pressure, and mode of heat transfer. Heat transfer takes place by convection, conduction, radiation [3**]**. Dehydration of food stuff requires gentle (< 60℃) temperatures and an even airflow. This process slowly removes the moisture from foods through evaporation. The process is sustained until more than 95% of moisture content in the food is removed. A properly dehydrated item is usually determined by physical inspection. An experienced hand and eye can easily detect a properly dehydrated item: through visual appearance and feel. Generally, such items will not feel moist, bend or be sticky. It will crunch or snap easily when an attempt is made to bend it [4**]**

The dehydrator is a device that has relatively few components required for its operation. Typical dehydrators have shelves, a heat source, a fan and a specially-designed housing that will permit flow of air across the drying chamber for effective removal of moisture. Studies show that every design of dryer is unique. Scalability – even for dryers of the same working principle – is very difficult. Even the simplest dryers have highly nonlinear characteristics. Hence, laboratory experimentation and pilot models – alongside field experience is required in the development of a new dryer (Jangam*et al*, 2010).Computerized technologies have been implemented to aid in the design process. Such computerized analytical technologies include FEA and CFD. These computational methods when correctly configured can provide designers with information on how a product will perform in real life. The information provided by such analysis can aid in improving product manufacturability, efficiency and safety standards [5**]**.

FEA is a computational technique that uses FEM to analyse any mathematical or physical problem that can be described using calculus. The object to be analysed is first modelled; then meshed. Boundary conditions are defined and applied; then the model is solved. The solution is post processed to provide interpretation for the observations made. CFD involves the analysis of fluid flows using numerical solution methods. It is the science of predicting flow of fluids, chemical reactions, heat and mass transfer or other related phenomena. This form of analysis complements experimentation and testing**[**6]

Energy demands vary from time to time throughout the day. TES systems have been developed to help in keeping thermal engines or devices running when the primary heat source is not available; or when the quantity available is not sufficient to run the system. In processes that involve emission of waste energy to the environment, such energy can be recovered; thereby leading to reduction in cost of running equipment with "premium fuels". TES systems work by storing energy in melting, heating, cooling, solidifying, or vaporizing a material. When the process is reversed, the thermal energy becomes available [7]

Drying is an important aspect of food processing. Without adequate removal of water from a food item, it will degrade and thereby become unsafe for consumption. Studies show that post-harvest losses of fruits and vegetables in developing countries are almost30% – 40% .Studies show that in comparison with designs that ensure air flow horizontally across the trays,conventional solar dehydrator designs are inefficient, because they have air inlet to the drying chamber mainly from the bottom, leading to uneven drying of food items and longer drying duration**[**8**]**,[3]..

Furthermore, existing solar thermal dehydrators are used outdoors – where it can receive solar power in sufficient quantity. The use of solar-thermal dehydrators poses some health risk :due to higher ambient temperature outside– especially during the peak hours of sunshine, the operator is exposed to unfavourable working conditions. This might seem arbitrary at a small scale, but if the dryer is large and there is need to work outdoors for a long time; the effect becomes more obvious.

Another challenge is in the aspect of insufficient research on solar dryer performance. As noted by **[**9**]** , unfortunately, existing solar dryer studies concentrate on modelling the drying of the fruits or vegetables; while paying less attention to the actual performance of the solar dryer. The existing solar dehydrators are inefficient, and inconvenient, leading to higher operational cost; therefore, this study was carried out to address these issue.

The objective of this research is to develop an optimized design of a solar dehydrator using computational techniques.

1.1 The Solar Resource

Energy in our solar system is produced mainly by the Sun. Solar power is responsible for sustaining life on earth. **[**10**]** note that energy comes to the organism from sunlight. Solar power and energy resources on our planet are enormous, eco-friendly and virtually inexhaustible. Solar energy drives other renewable energy sources such as wind, hydropower, animal power and biomass. Outside our atmosphere, the intensity of solar power is more than 1kW/m^2 emitted continuously. On the earth's surface, the average daily interception of this enormous amount of power is 4 kWh/m^2. The amount of solar energy intercepted in less than one month by the earth is equivalent of all the energy that is originally stored in coal, natural gas and petroleum available on the planet.

The solar constant – the amount of energy arriving the earth's atmosphere from the sun – is approximately 1367 W/m^2. This amount varies over time due to variations caused by solar flares and sun spots[10]

Due to constraints arising from absorption and diffraction of the sunlight in the earth's atmosphere, variations in weather, loss of sunlight at night, the amount of solar energy (average insolation) reaching a given location on earth is lower than the amount outside the atmosphere.

1.2 Solar Thermal Energy Systems

For thousands of years – since mankind began interacting with inanimate objects in search for comfort, solar heat has been used in various forms for different purposes. Such purposes include for space and water heating, cooking, and electricity generation. Although solar power on earth on a daily basis is enormous, its availability is not instantaneous at all times and seasons. Also, it is not useful at large scale at several locations on earth. For this reason, it must be captured at suitable temperature, transported and possibly stored for later use [10].

Open sun drying is one of the oldest forms of preserving agricultural produce is by spreading it in the sun for several hours for water to evaporate from it. Although still practiced in many parts of the world today, it is saddled with lots of disadvantages; namely: exposure to insects, rodents and livestock, dust contamination, long drying duration and low quality of produce [11] [9].

Solar heating is widely applied in crop drying in agriculture, in water and space heating, growing food in greenhouses, producing salt from evaporated sea water, cooking and electricity generation. The solar heat is available in nature as diffuse and temporarily available. There is no location on earth that receives solar power in a continuous and predictable quantity. Such is only possible in space. It therefore requires large collection areas to capture sufficient heat energy and convert same to heat. The heat captured is sometimes stored in thermally insulated enclosures until when needed. Such storage facilities are designed with effective controls to prevent waste of the energy captured **[**10**]**

Solar collectors include: Stationary (Non-Concentrating) Solar Collectors, flat plate solar collectors, evacuated-tube solar collectors, concentrating collectors, parabolic trough

solar collectors, non-imaging solar concentrators, dish solar collectors and central receivers.

Table 1 gives a summary of solar collectors and their operating temperature range as well as the control.

Table 2.1: Solar Energy Collectors

Motion	Collector Type	Absorber Type	Concentration Ratio	Indicative Temperature Range (℃)
Stationary	Flat-plate collector (FPC)	Flat	1	30 – 80
	Evacuated tube collector (ETC)	Flat	1	50 – 200
	Compound parabolic collector (CPC)	Tubular	1 – 5	60 – 240
Single-axis tracking	Compound parabolic collector (CPC)	Tubular	5 – 15	60 – 300
	Linear Frensel reflector (LFR)	Tubular	10 – 40	60 – 250
	Cylindrical trough collector (CTC)	Tubular	15 – 50	60 – 300
	Parabolic trough collector (PTC)	Tubular	10 – 85	60 – 400
Two-axis tracking	Parabolic dish reflector (PDR)	Point	600 – 2000	100 – 1500
	Heliostat field collector (HFC)	Point	300 – 1500	150 – 2000

Note: Concentration ratio is the aperture area divided by the receiver/absorber area of the collector

[12]

Food Dehydrators include: Solar Food Dehydrators, Directional Flow Characteristics in Food Dehydrators.

Table 2 shows a comparison between vertical and horizontal food dehydrators.

Table 2: **Comparison between Vertical and Horizontal Food Dehydrators**

S/N	Vertical Air flow Food Dehydrators	Horizontal Food Dehydrators
1	Airflow originates from the bottom to the top of the dehydrator	Air flows from the rear of the dehydrator to the front.
2	Mostly stackable	Not stackable
3	Tend to dry food on the lower trays faster than on the upper trays	Uniform drying of food items
4	Food flavours may be mixed as air passes from one level of food to another	No contamination in flavours
5	Base mounted fan-heater configuration can be polluted by food particles	Less vulnerable to problems caused by food ingress to the fan-heater unit
6	Difficult to load and offload the trays	Easy loading and offloading of the trays

[8]

1.3 CFD Analysis

The analysis for food drying analytically is a complex process. Drying can be characterized as a combined multiscale. Multiphysics problem. CFD modelling and simulation is very important in the study of solar dryers. However, very few studies have been conducted in this aspect. Also, studies have been conducted immensely on CFD modelling and simulation of fruits and vegetables at a micro level, without considering actual performance of the solar dryer. However, the performance of a solar dryer has immense impacts on the quality of the food item being dried **[**13].Generally, [9] notes that, CFD involves the use of numerical methods and computer algorithms to analyse and solve problems involving fluid flows. It provides insight into flow patterns that are expensive, difficult or virtually impossible to study using traditional (experimental) techniques, such as wind tunnel studies. The procedure for CFD analysis is shown in Figure 1.

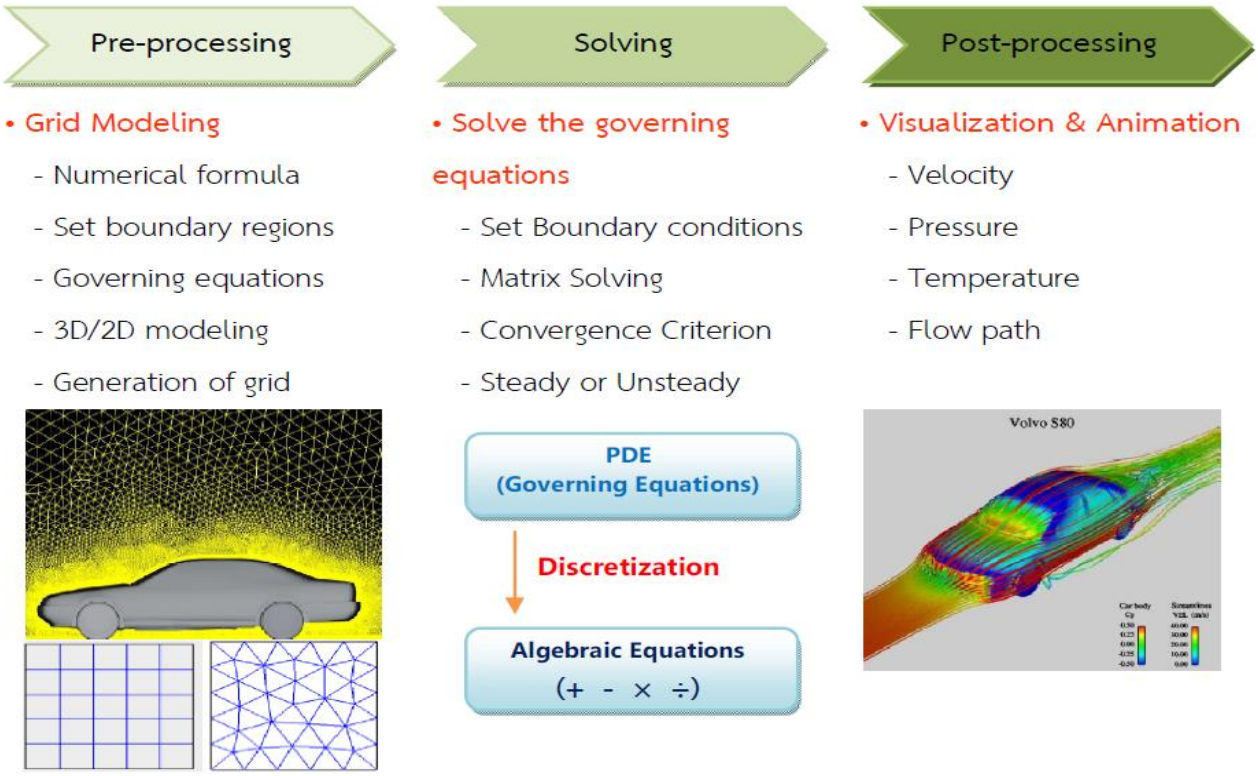

Figure 1: **The CFD Process [14]**

Although CFD has become a remarkably useful tool in product development, it does not replace the need for experimentation. Table 3 shows the comparison developed by [4] between experiments and simulations.

Table 2: Comparison between Experiments and Simulations

Experiments	Simulations
Involves physical (quantitative) measurements of flow phenomena	Involves quantitative prediction of flow phenomena using a CFD software
One quantity is measured at a time	All desired quantities can be measured simultaneously
Measurements are taken at a limited number of points and time instants	Analysis is carried out with high resolution in space and time
Usually developed for a laboratory-scale model	Can be designed for virtually any problem at realistic operating conditions
Sources of error include: measurement errors, flow disturbances by probes, etc	Sources of error include: modelling, discretization, iteration and implementation
Experiments can be expensive and slow	Simulations are cheaper and faster
Experiments are sequential and single-purpose	Simulations are parallel and multi-purpose

Source: [14]

1.4 Working with FEA

Modern engineering has been greatly enhanced by developments in computer technology. At present, virtually all aspects of engineering design process have been computerized. FEA is based on the principle of simplifying a complicated object to make it easier to analyse. The idea of 'simplifying' an object implies discretization. FEA makes it possible to virtually test a product design by subjecting it to loading (mechanical, thermal or electromagnetic). The study can be applied in different fields of study including fluid flow, heat transfer, electrostatics or electromagnetics and structural or solid mechanics[15]. The procedure for carrying out FEA are as follows:

1. Create the geometry.
2. Apply mesh to the geometry (a collection of elements and nodes).
3. Describe how physical quantities interact with each element.
4. Assemble the elements at the nodes to form an approximate set of equations for the entire model.
5. Apply boundary conditions and loads.
6. Solve the system of equations
7. Calculate the required quantities and visualize (post-processing)

Several studies have been conducted on solar dryers and food dehydration. However, no study reviewed examines a comparative effect of hot air flow direction from the bottom and the backof the dehydrator in to the drying chamber. Heretofore, the heat and flow distribution resulting in uniform

(or non-uniform) drying of product in the device. Although a few computational studies have been carried out on the mechanics of food drying in a solar dehydrator, computational techniques implemented do not consider the effect that the design of the solar dehydrator have on its performance. This study aims at addressing these issues.

2.0 MATERIALS AND METHODS

The materials that was used in this study include computer hardware and software. Software that were used include AutoCAD 2016, ANSYS 17.2 and MATLAB R2020a. AutoCAD was used in developing the 2D sketches and solid models. This was further processed in ANSYS Design Modeller. The ANSYS package contains software for pre-processing, analysis and post-processing the model to be studied. MATLAB R2020a was used to analyse the heat exchanger system for the dehydrator. Figure 2 shows a schematic model of solar dehydrator system designed for this research, Figure 3 shows part of designed solar dehydrator.

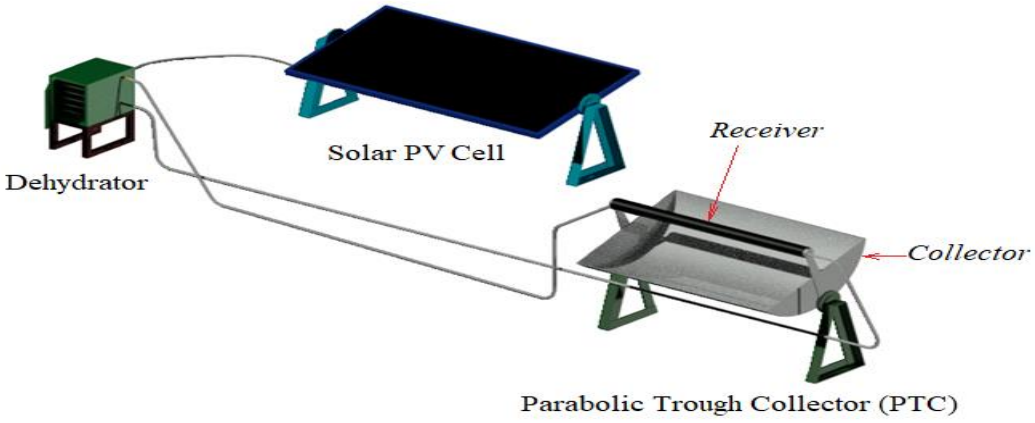

Figure 2: **Schematic Model of the Solar Dehydrator System**
Source: Researcher

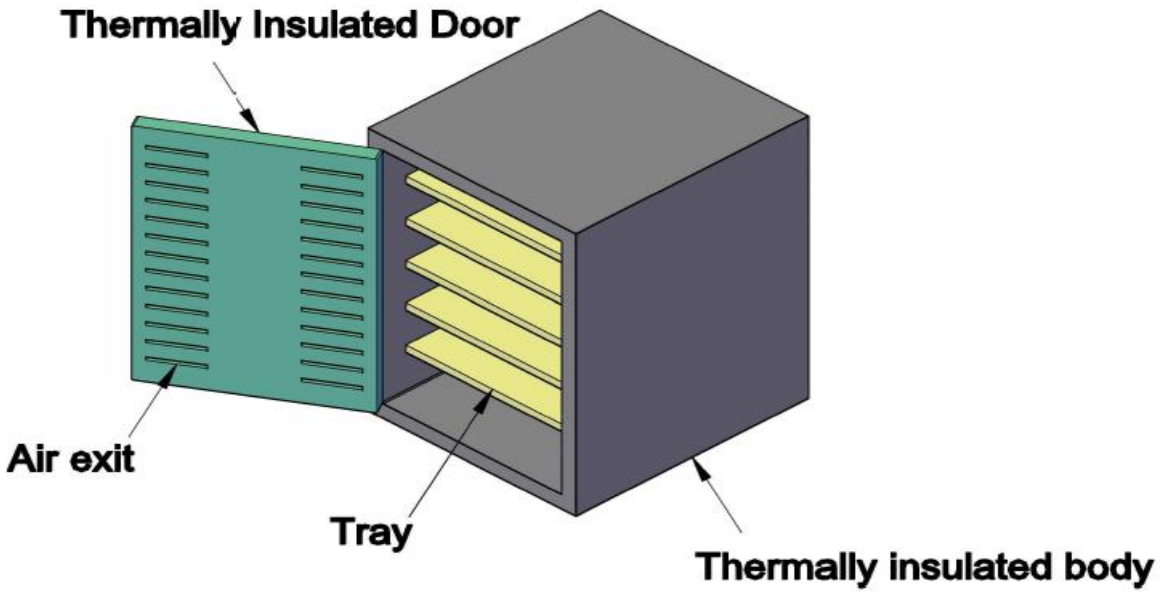

Figure 3: Parts of the Dehydrator Designed for this Study
Source: Researcher

2.1 Design of the Solar Collector and Heat Exchanger

The solar collector in the dehydrator system is designed to capture solar heat and transmit the heat to a working fluid; which in turn is used to feed a heat exchanger – where the air is heated by the hot fluid and moved to the drying chamber. A parabolic trough collector (PTC)was selected for this analysis. Table 3 shows the parameters used in this analysis. The data and module used for this work is based on the work of [16]. This was a necessary choice since their model has been empirically tested and validated.

Table 3: Parameters for the PTC

Parameter	Symbol	Value
Width of the collector	W	5.0 m
Length of the collector	L	7.8 m
Focal distance of the collector	f	1.71 m
Aperture of the collector	A_a	39.0 m^2
Concentration ratio of the collector	C	22.74
Receiver inner diameter	D_{ri}	66×10^{-3}m
Receiver outer diameter	D_{ro}	70×10^{-3} m
Cover inner diameter	D_{ci}	109×10^{-3} m
Cover outer diameter	D_{co}	115×10^{-3} m
Receiver inner surface	A_{ri}	1.617 m^2
Receiver outer surface	A_{ro}	1.715 m^2
Cover inner surface	A_{ci}	2.671 m^2
Cover outer surface	A_{co}	2.818 m^2
Receiver emittance	ε_r	0.2
Cover emittance	ε_c	0.9
Absorber absorbance	α	0.96
Cover transmittance	τ	0.95
Concentrator reflectance	ρ_c	0.83
Intercept factor	γ	0.99
Incident angle modifier (zero incident angle)	$K(\theta = 0^o)$	1
Incident angle	θ	0^o
Maximum optical efficiency (zero incident angle)	$\eta_{opt,\,max}$	75%

[14]

The working fluid used in the PTC is Syltherm 800. Data sheet for the working fluid was published by [17].

Assumptions:

The following assumptions were made in modelling the collector:

i. The collector surface is gray i.e. radiation properties are independent of wavelength.
ii. The incident energy over the collector surface is uniform
iii. The collector transmits thermal energy to the receiver and the ambient predominantly by radiation.
iv. The thermal flux over the absorber is uniform.
v. Contact thermal losses are negligible
vi. The collector operates in steady-state conditions.
vii. There is no variation in temperature along the receiver.
viii. Due to the vacuum between the receiver and its glass cover, heat loss by convection in the receiver tube is negligible.
ix. There is infinitesimal difference in temperature between the receiver and the fluid.
x. Thermal losses at the contacts are negligible.

Considering the relative sizes of the receiver cover and the tube containing the working fluid, the glass cover is typically larger in surface area. Thus, we can consider the receiver tube as a small convex object surrounded by a large surface. Consequently, applying the equation for heat transfer by radiation between both surfaces as noted in [18]. Equation 1 can be expressed as follows:

$$Q_{loss} = A_{ro} \times \varepsilon_t \times \sigma \times \left(T_r{}^4 - T_c{}^4\right) \quad .1$$

where: A_{ro} is the area of the receiver outlet
ε_t is emissivity of the receiver (equivalent emittance)
σ is Stefan-Boltzmann constant
T_r is temperature of the receiverpipe
T_c istemperature of the evacuated glass cover
But, ε_t is given by:

$$\varepsilon_t = \left[\frac{1}{\varepsilon_r} + \frac{1-\varepsilon_c}{\varepsilon_c} \times \frac{A_{ro}}{A_{ci}}\right]^{-1} \quad 2$$

If we consider the effective heat loss by both the collector and receiver to the surrounding, Equation 3.1 becomes:

$$Q_{loss} = A_{ro} \times \varepsilon_t \times \sigma \times \left(T_r{}^4 - T_{am}{}^4\right) - A_{ro} \times \varepsilon_t \times \sigma \times \left(T_c{}^4 - T_{am}{}^4\right) \quad .3$$

According to [18], heat loss from the housing of the collector to the surroundings is given by Equation:

$$Q_{loss} = \left[A_{co} \times \varepsilon_c \times \sigma \times \left(T_c{}^4 - T_{am}{}^4\right)\right] + \left[A_{co} \times h_{out} \times (T_c - T_{am})\right] \quad 4$$

Due to the existence of an evacuated tube collector, the cover temperature may be assumed to be close to the ambient temperature. Therefore, Taylor series can be applied to rewrite Equation 2 as follows.

$$T_c{}^4 - T_{am}{}^4 \approx 4 \times T_{am}{}^3 \times (T_c - T_{am}) \quad 5$$

Using Equation 3, Equation 2 can be rewritten as shown in Equation 4.

$$Q_{loss} = \left[A_{co} \times \varepsilon_c \times \sigma \times 4 \times T_{am}{}^3 \times (T_c - T_{am})\right] + \left[A_{co} \times h_{out} \times (T_c - T_{am})\right] \quad 6$$

$$= \left[A_{co} \times \varepsilon_c \times \sigma \times 4 \times {T_{am}}^3 + A_{co} \times h_{out}\right] \times (T_c - T_{am})$$

7

Let

$$K_1 = A_{co} \times \varepsilon_c \times \sigma \times 4 \times {T_{am}}^3 + A_{co} \times h_{out}$$

8

$$\therefore Q_{loss} = K_1 \times (T_c - T_{am})$$

9

Referring to Equations 3.5 and 3.9, we can re-write Equation 3.4 as follows:

$${T_c}^4 - {T_{am}}^4 = \frac{4 \times {T_{am}}^3}{K_1} \times Q_{loss}$$

10

Thus, with Equations 3.3 and 3.10, we have:

$$Q_{loss} = A_{ro} \times \varepsilon_t \times \sigma \times \left({T_r}^4 - {T_{am}}^4\right) \times \left[1 + \frac{4 \times {T_{am}}^3 \times A_{ro} \times \varepsilon_t \times \sigma}{K_1}\right]^{-1}$$

11

Let

$$K_2 = A_{ro} \times \varepsilon_t \times \sigma \times \left[1 + \frac{4 \times {T_{am}}^3 \times A_{ro} \times \varepsilon_t \times \sigma}{K_1}\right]^{-1}$$

12

But, heat transferred to the working fluid is given by:

$$Q = A_{ri} \times h \times \left(T_r - T_{fm}\right)$$

13

where: A_{ri} is the area of the inner surface of the pipe conveying the working fluid,

h is heat transfer coefficient between the fluid and absorber, W/m^{2}K

T_r is receiver temperature

T_{fm} is mean fluid temperature

$$T_{fm} = \frac{T_i + T_o}{2}$$

14

T_i is fluid inlet temperature

T_o is fluid outlet temperature

Equation 13 can also be expressed in terms of the heat transferred to the working fluid as shown in Equation 15

$$Q_u = \dot{m} \times c_p \times (T_o - T_i)$$

15

where: $\dot{m}$ is the mass flow rate of water, kg/s; it is calculated as shown in Equation 3.16.

$$\dot{m} = \rho V$$

16

where: ρ is the density of water

V is volumetric flow rate (m^3/s)

c_p is specific heat capacity at constant pressure, J/kg K

Furthermore, according to [18], the useful heat transferred to the working fluid can be computed with Equation 3.17.

$$Q_u = \left[\frac{1}{A_{ri} \times h} + \frac{1}{2 \times \dot{m} \times c_p}\right]^{-1} \times (T_r - T_i)$$

17

Let

$$K_3 = \left[\frac{1}{A_{ri} \times h} + \frac{1}{2 \times \dot{m} \times c_p}\right]^{-1}$$

18

Hence, Equation 3.16 can be rewritten as shown in Equation 3.19

$$Q_u = K_3 \times (T_r - T_i)$$

19

But, not all the energy available for useful work came from the solar insolation. Some losses are expected; hence we talk about the efficiency of the collector. Thermal efficiency (η_{th}) of the collector is given as follows.

$$\eta_{th} = \left[\eta_{opt} \times \left(1 + \frac{4 \times T_i \times K_2}{K_3}\right)^{-1}\right] - \left[K_2 \times \left(1 + \frac{4 \times T_i \times K_2}{K_3}\right)^{-1}\right] \times \frac{({T_{in}}^4 - {T_{am}}^4)}{A_a \times G_b}$$

.20

Let

$$K_4 = \left[\eta_{opt} \times \left(1 + \frac{4 \times T_i \times K_2}{K_3}\right)^{-1}\right]$$

21

And

$$K_5 = \left[K_2 \times \left(1 + \frac{4 \times T_i \times K_2}{K_3}\right)^{-1}\right]$$

22

Thus, re-writing Equation 3.20, we have:

$$\eta_{th} = K_4 - K_5 \times \frac{({T_{in}}^4 - {T_{am}}^4)}{A_a \times G_b}$$

23

Also, the effective thermal loss (Q_{loss}) in the solar collector is calculated using Equation 3.24.

$$Q_{loss} = \left(\eta_{opt} - K_4\right) \times Q_s + K_5 \times \left({T_{in}}^4 - {T_{am}}^4\right)$$

24

where: η_{opt} is the optical efficiency. This is calculated as shown in Equation 25

$$\eta_{opt}(\theta) = K(\theta) \times \eta_{opt,max}$$

25

where: θ is the incident angle (in degrees)

$K(\theta)$ is incident angle modifier.

$\eta_{opt,max}$ is maximum optical efficiency which is calculated as shown in Equation 26.

$$\eta_{opt,max} = \rho_c \times \gamma \times \tau \times \alpha$$

26

ρ_c is the concentrator reflectance

γ is intercept factor

τ is cover transmittance

α = absorber absorbance

Furthermore, the solar thermal flux (Q_s) is calculated with Equation 27.

$$Q_s = \frac{Q_u + Q_{loss}}{\eta_{opt}}$$

27

The fluid outlet temperature (T_o) can be calculated with Equation 28.

$$T_o = T_{in} + \frac{K_4}{\dot{m}\times c_p} \times Q_s - \frac{K_5}{\dot{m}\times c_p} \times \left({T_i}^4 - {T_{am}}^4\right) \quad .28$$

To calculate the temperature of Syltherm 800 at the inlet of the heat exchanger, we need to consider the heat transfer from the PTC to the heat exchanger. The heat exchanger is the unit in the dehydrator setup that transfers heat from the solar collector to the drying chamber. In its analysis, the following assumptions were made:

i. Flow is hydrodynamically and thermally fully developed
ii. Velocity and temperature are uniform over the cross section of the pipe.
iii. Heat loss through the fluid transfer pipe is negligible – due to lagging.
iv. Physical properties of the fluid are also time-independent.

The rate of heat transfer from the PTC to the heat exchanger was calculated using Equation 29.

$$Q = UA\Delta T = UA(T_1 - T_2) \quad 29$$

where A is surface area of the pipe (in m^2)

$$A = \pi L(d_o + d_i) \quad .30$$

T_2 is temperature of the hot fluid leaving the collector (in K)
T_2 is temperature of fluid on the other end of the pipe (in K)
U is the overall heat transfer coefficient (in W/m^2K)

But, $U = \frac{1}{R_f + R_i + R_o}$ 31

where:R_f is the thermal resistance of the pipe insulation (k/W)
R_i is thermal resistance of the inside surface of the pipe (k/W)
R_o is thermal resistance of the outside surface of the pipe (k/W)
Mathematically,

$$R_f = \frac{ln(r_o/r_i)}{2\pi k_f L} \quad 32$$

where: r_o and r_i are the outside and inside radii of the pipe (in m)
L is length of the pipe (m)
$k_f$is thermal conductivity of the insulation material (in W/m.K)

Similarly, $R_i = \frac{1}{h_i A}$ 33

where: h_i is the convective heat transfer coefficient on the inside of the pipe (in W/m^2K)

$$h_i = \frac{Nu_i k_i}{d_i} \quad 34$$

where: Nu_i is the Nusselt number for internal flow
k_i is the thermal conductivity of Syltherm 800 (in W/m.k)

Also, $R_o = \frac{1}{h_o A}$ 35

where:h_o is the convective heat transfer coefficient on the outside of the pipe (in W/m^2K)

$$h_o = \frac{Nu_o k_f}{[d_o \ln(r_o/r_i)]} \quad 36$$

where: Nu_o is the Nusselt number for external flow

$$Nu_o = \left((0.63(d_o/d_i))^{0.33}\right) \times \left((m/(d_i \pi c_p))^{0.4}\right) \times \left((k_l/k_f)^{0.1}\right) \quad .37$$

The heat exchanger selected for this application was a single row cross-flow heat exchanger. The hot Syltherm 800 flows through a copper tube. The tube has aluminium fins installed on it to provide a larger surface area for heat exchange with air flowing through it from the surrounding. The heat exchanger was designed as a compact unit for transferring heat from the hot Syltherm 800 into the air flowing into the dryer from the surrounding using an axial fan capable of generating airflow between 1 m/s and 5 m/s. The temperature of air leaving the heat exchanger was calculated using Equation 38.

$$T_{out} = T_{fin} - \frac{Q_{air}}{\left(\frac{K_{al}}{A_{fin}} + h_{air}\right)} \quad 38$$

where: T_{fin} is temperature of the fins on the heat exchanger
Q_{air} is heat flux in the air
K_{al} is thermal conductivity of aluminium (the fin material) (in W/m.K)
A_{fin} is Area of the fin (in m^2)
h_{air} is convective heat transfer coefficient between the fins and air (W/m^2. K)
Figure 4 shows a 3D model of the heat exchanger.

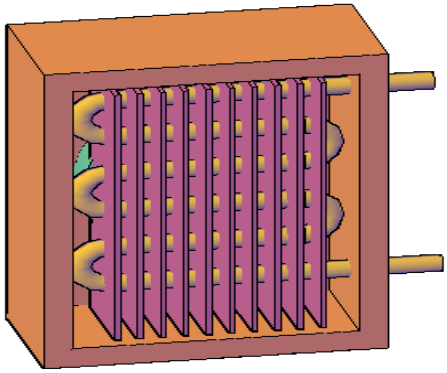

Figure 4: 3D Model of the Heat Exchanger
Source:
Researcher

But, $T_{fin} = T_{in} - \frac{\dot{V}}{\rho c_p} \times \frac{h_{tube} A_{tube}(T_{in} - T_{out})}{A_{total}}$ 39

where: T_{in} is the inlet temperature of the fluid (in K)
$\dot{V}$ is volume flow rate (in m^3/s)

ρ is density of the fluid (in kg/m^3)
c_p is specific heat of the fluid (in J/kg.K)
h_{tube} is convective heat transfer coefficient between the tube and fluid
A_{tube} is surface area of the tube (in m^2)
A_{total} is total surface area of the tube (in m^2)

Also, $h_{tube} = \frac{N_u k_{cu}}{D_{tube}}$ 40

where: N_u is the Nusselt number obtained using the Churchill and Bernstein correlation given in Equation 41 [19].
k_{cu} is the thermal conductivity of copper (in W/m.K)

$Nu = 0.023 {Re_d}^{4/5} \times 0.8^{-1/5}$ 41

The Reynold's number was calculated based on the tube diameter as shown in Equation 42.

$Re_d = \frac{4\dot{V}}{\pi \rho D}$ 42

Also, $Q_{air} = \frac{h_{air} A_{fin}}{T_{fin} - T_{out}}$ .43

The Equations for the design of the PTC and the heat exchanger were implemented using MATLAB software

2.2 Computational Model of the Dehydrator

The development of computer technology has facilitated electronic development and analysis of computational models of complex geometries. Computers with high computing powers have been able to solve the three-dimensional Navier-Stokes equations. CFD is an emerging field in engineering, but has greatly reduced expenses incurred in product development.CFD was chosen over FEA for this study due to the fact that FEA is not really designed to handle the strong convection typical in the analysis of fluid flow. This defect in FEA solution leads to convergence and stability problems in thermo-fluid simulation problems. FEA is more suited for structural analysis, but can be used to solve some fluid problems. In contrast, CFDis stable and effectively handles the convection term (highlighted) found in the general Navier-Stokes Equation [20].

$$\rho\left(\frac{\partial \boldsymbol{u}}{\partial t} + \boldsymbol{u} \cdot \nabla \mathbf{u}\right) = -\nabla p + \nabla \cdot [\mu(\nabla \boldsymbol{u} + (\nabla \boldsymbol{u})^T)] + \nabla \cdot [\lambda(\nabla \cdot \boldsymbol{u})\mathrm{I}] + \rho g \quad 44$$

In this section, the key elements in the modelling and simulation of the dehydrator is discussed.

2.2.1 The Computational Domains

The solid models for this study were created in six configurations using AutoCAD software. The drawing files were then imported to Ansys Design Modeller through the Workbench. After necessary tuning of the solid geometry, the computational domains were created using advanced Boolean operations in the Design Modeller. The result of this step was exported to the Ansys Meshing Module.

2.2.2 Mesh Generation

In the Ansys meshing module, the faces of the computational domain were defined. This step was necessary to prepare the solid model for subsequent definition of boundary conditions in Fluent. The source of thermo-flow was defined as velocity inlet. The outflow portions (the red-highlighted projections on the solid models) were defined as pressure outlet; and all other parts of the computational domain was declared to be thermally-insulated walls. Figures 5 to 10 show different meshed configurations of the dehydrator studied.

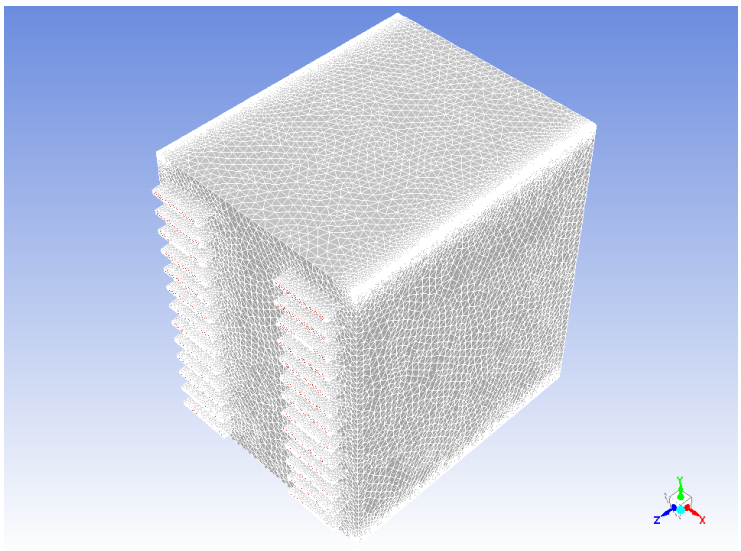

Figure 5: Dehydrator with Back Inflow and Front Outflow

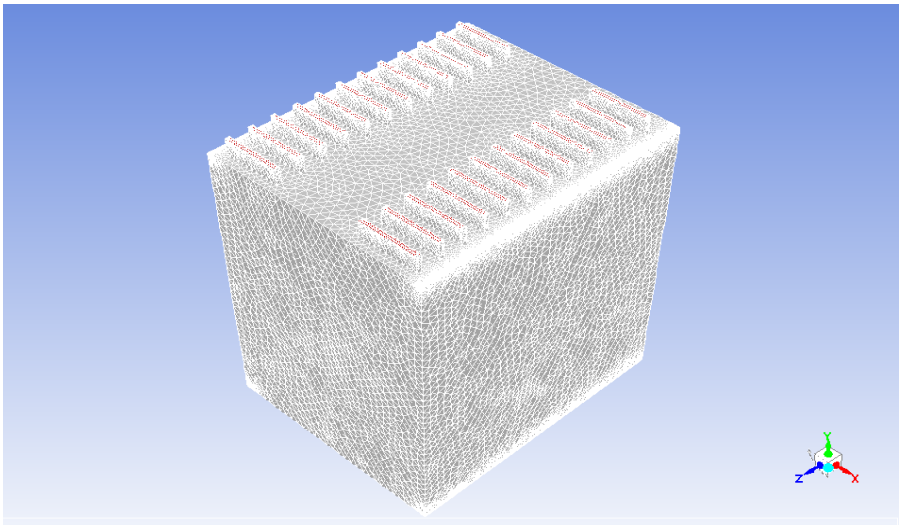

Figure 6: Dehydrator with Back Inflow and Top Outflow

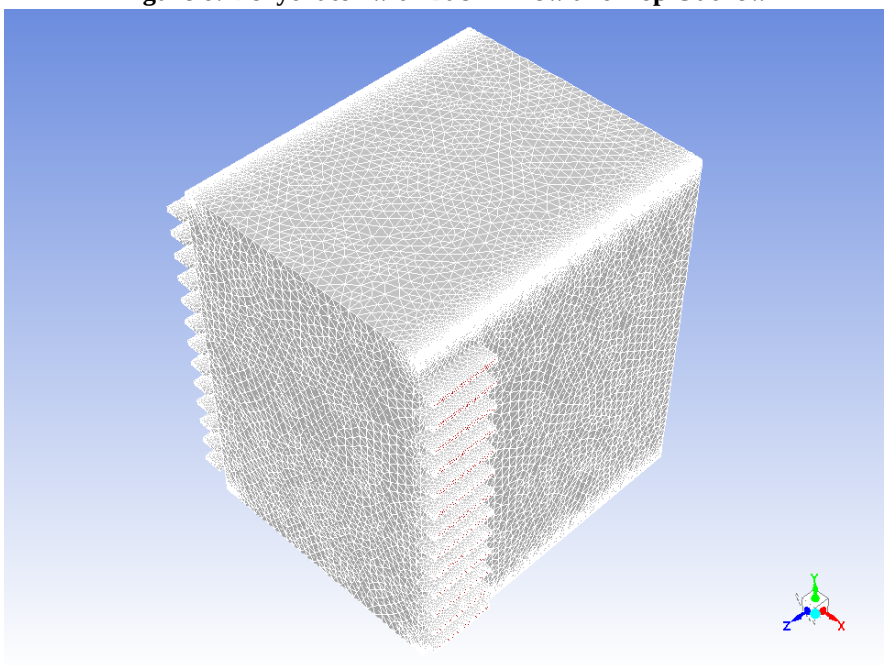

Figure 7: Dehydrator with Back Inflow and Sides Outflow

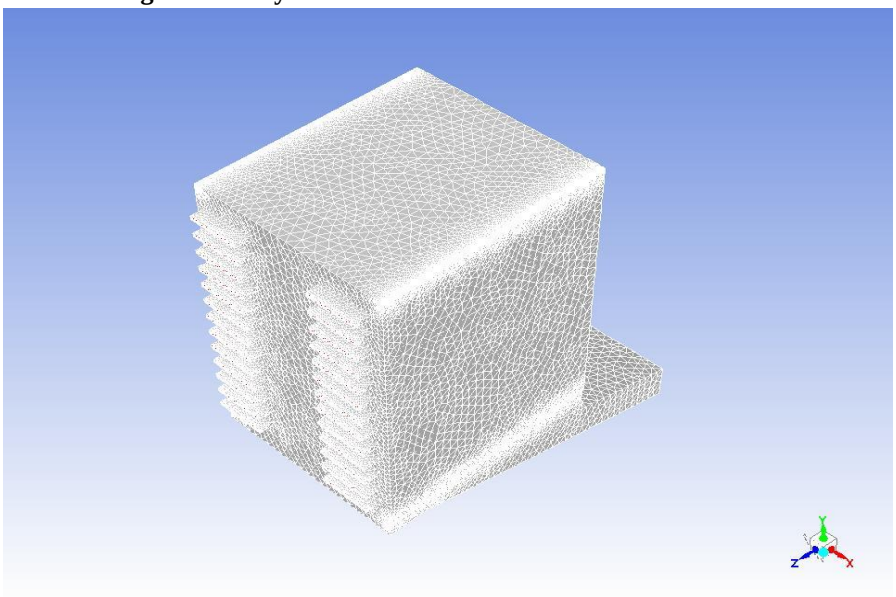

Figure 8: Dehydrator with Bottom Inflow and Front Outflow

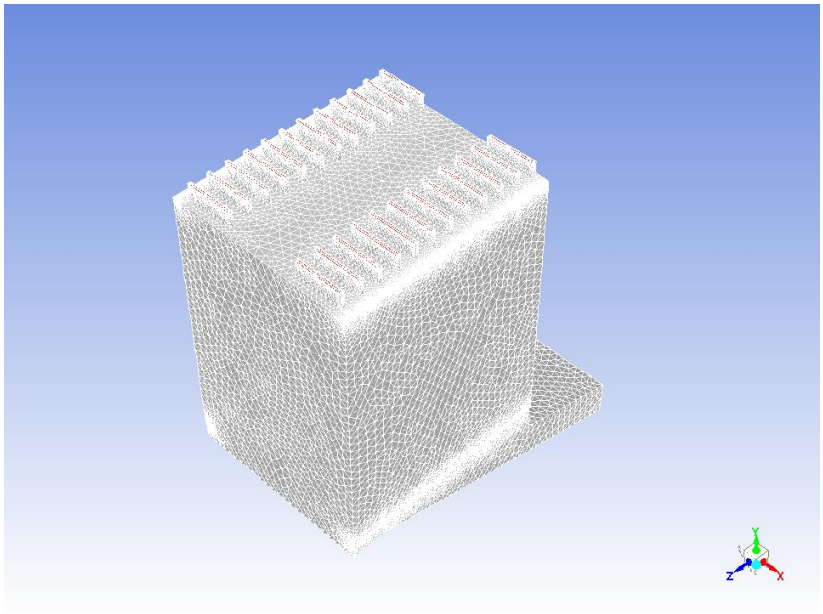

Figure 9: Dehydrator with Bottom Inflow and Top Outflow

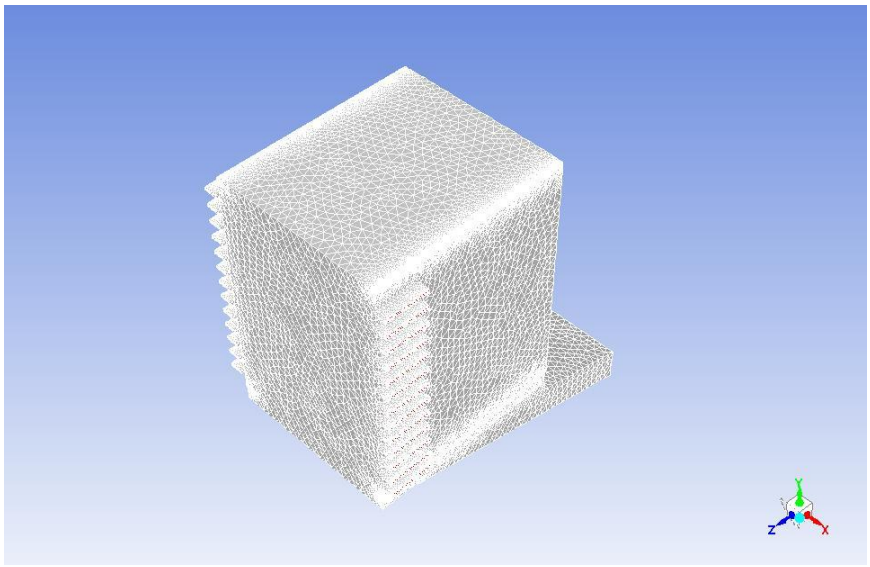

Figure 10: Dehydrator with Bottom Inflow and Sides Outflow

The meshes were tetrahedral-structured. Table 4 gives a summary of the number of nodes and elements that made up each of the configurations studied.

Table 4: Number of Nodes and Elements for Each Configuration of the Dehydrators

Configuration	Number of Nodes	Number of Elements
Back inflow; front outflow	161786	795034
Back inflow; top outflow	159639	787232
Back inflow; sides outflow	159810	783736
Bottom inflow; front outflow	151779	759417
Bottom inflow; top outflow	158272	794046
Bottom inflow; sides outflow	157526	786814

For precision in calculation, the meshes were refined at the air exits as shown in Figure 11.

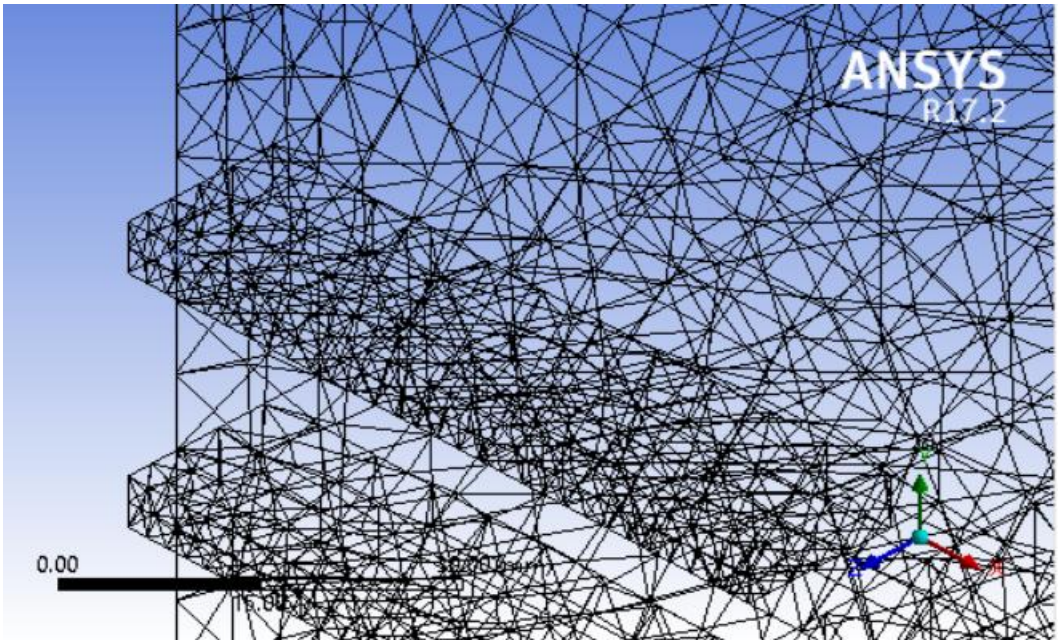

Figure 11: Mesh Refinement at the Outlets

2.3 Governing Equations

The drying kinetics and CFD modelling were done based on thermal and hydrodynamic models. The governing equations in this study include the continuity equation, energy equation, mass transfer, and turbulence models. These are shown in Equations 45 to 48.

The flow of any fluid can be described using the Navier-Stokes transport equations. The equations are formulated by considering momentum, energy and mass balances in an infinitesimal element of fluid which results in a set of partial differential equations.

For continuity, $\frac{\partial \rho}{\partial t} + \nabla(\rho \vec{u}) = 0$ 45

where: $\vec{u}$ and ρ are velocity and density of air respectively

Also, for the momentum,

$\frac{\partial(\rho E)}{\partial t} + \nabla.\left(\vec{u}(\rho E + P)\right) = \nabla.(-\vec{q} + \bar{\bar{\tau}}.\vec{u}) + S_h$ 46

where: S_h, $\vec{q}$ and E are heat source term, heat flux vector and total energy respectively. The total energy in the system is the summation of internal energy and kinetic energy; given by:

$E = h - \frac{P}{\rho} + \frac{u^2}{2}$ 47

where: h is the sensible enthalpy of air

For mass transfer, in solar dehydrators, water vapour is analysed as a scalar property; thus, it does not alter the solutions of mass, momentum and energy for dry air. The mass transport of the scalar property is solved independently with a general conservation equation:

$\frac{\partial(\rho w)}{\partial t} + \nabla.(\rho \vec{u} w) = \nabla.(\rho D) + S_w$ 48

where w is the humidity ratio (kg water of vapour/kg of dry air)

D is the water vapour diffusion coefficient which depends on temperature.

In CFD modelling, the effect of turbulence flow is predicted using different turbulence models, namely: standard k-ε model, RNG k-ε model, realizable k-ε and Reynolds Stress Model (RSM). In this study, the RNGk-ε turbulence model was used; since it is widely validated and commonly used.

2.4 Boundary Conditions and Calculations

The Navier-Stokes equations were solved in Fluent using a pressure-based, steady-state configuration. In the Fluent software, air was defined as the fluid material in the computational domain. The exterior surfaces of the computational domain were defined as walls. The regions around the trays were also defined in the program as wall; with no-slip boundary conditions assigned. The thermo-flow inlet was defined as velocity-inlet boundary condition. The inlet velocity of air was set to 2 m/s. To account for the heat supplied to the air from the heat exchanger, the energy equation option was activated in the Fluent solver. This setting allows heat to be added to the system. The inlet air temperature was set to 350K in the fluid inlet boundary. The outlet boundaries were sent to pressure outlet, with no value of pressure pre-defined. This would be computed by the computer during the solution process. These conditions were used in all the six configurations that were analysed. Figure 12 shows part of the project schematic for this work as applied in the Ansys Workbench.

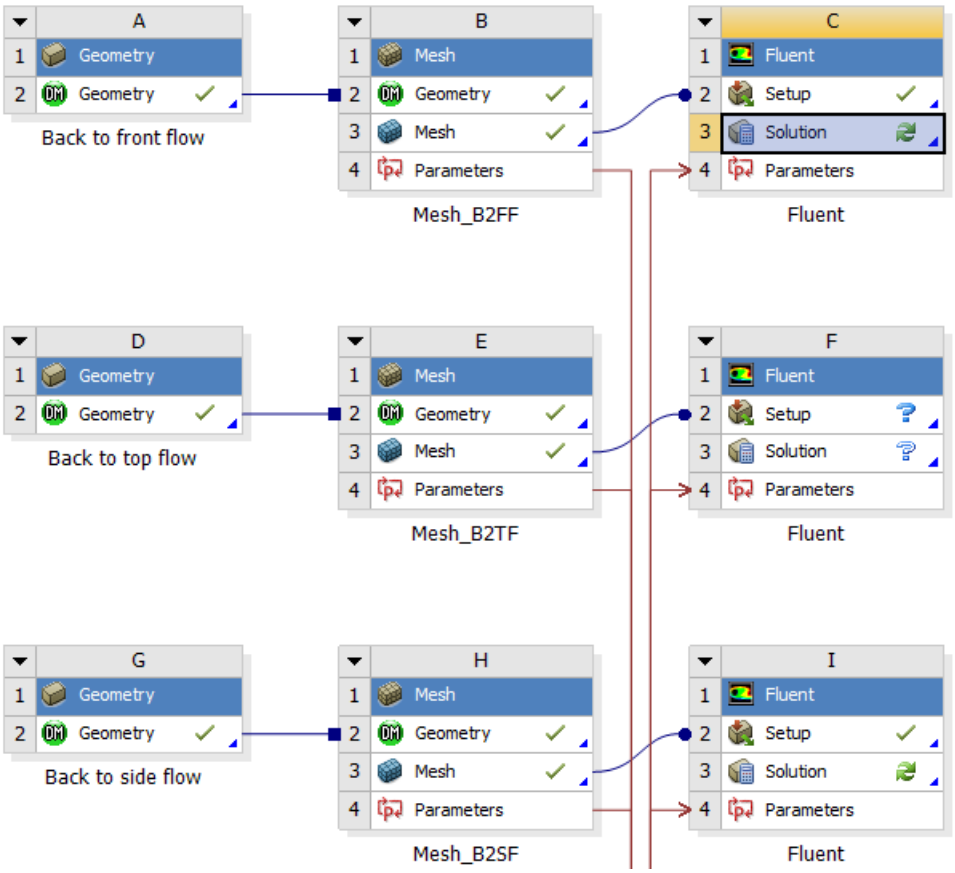

Figure 12: Project Schematic for the CFD Analysis on Ansys Workbench

3.0 RESULTS AND DISCUSSION

3.1 Results

The results of the design and analyses carried out in this research are presented in this chapter. Results for the solar collector design and heat transfer to the working fluid were obtained from the MATLAB program. CFD results on the other hand were obtained from post-processing the results produced in the Ansys Fluent CFD analysis.

3.1.1 Solar Collector and Heat Exchanger Results

The relationship between the temperature of Syltherm 800 at the outlet of the PTC, ambient temperature and mass flow rates were assessed. Figure 13 shows a surface plot between the variables.

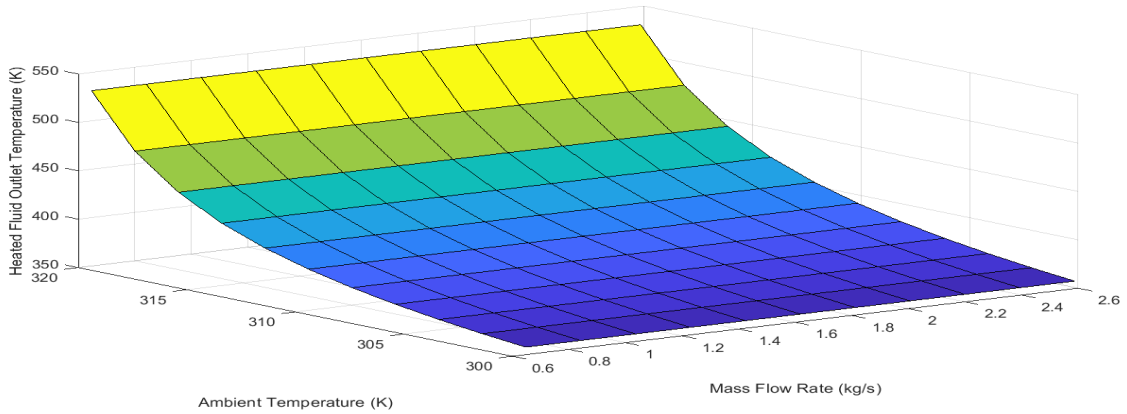

Figure 13: A Plot of the Temperature of Syltherm 800 PTC at the Outlet in Relation to Ambient Temperature and Mass Flow Rate

The inlet temperature of Syltherm 800 at the inlet of the heat exchanger and was also assessed in relation to the temperature of air leaving the heat exchanger. The result of the investigation is presented in Table 5. Figures 14 to 17 show the results obtained from the assessment of the relationship between the heated fluid and the air flow in the heat exchanger.

Table 5: Output Data for the Solar Collector and Heat Exchanger Design

HE Inlet Temperature (K)	Hot Air Temperature (K)	Syltherm 800 Collector Outlet Temperature (K)	Volume Flow Rate (m^3/s)	Heat Flux (W)
358.00	350.82	357.98	0.05	81.06
362.20	354.94	362.18	0.10	86.31
366.40	359.05	366.38	0.15	91.56
370.60	363.17	370.58	0.20	96.81
374.80	367.28	374.78	0.25	102.06
379.00	371.40	378.98	0.30	107.31
383.20	375.52	383.18	0.35	112.56
387.40	379.63	387.38	0.40	117.81
391.60	383.75	391.58	0.45	123.06
395.80	387.86	395.78	0.50	128.31
400.00	391.98	399.98	0.55	133.56

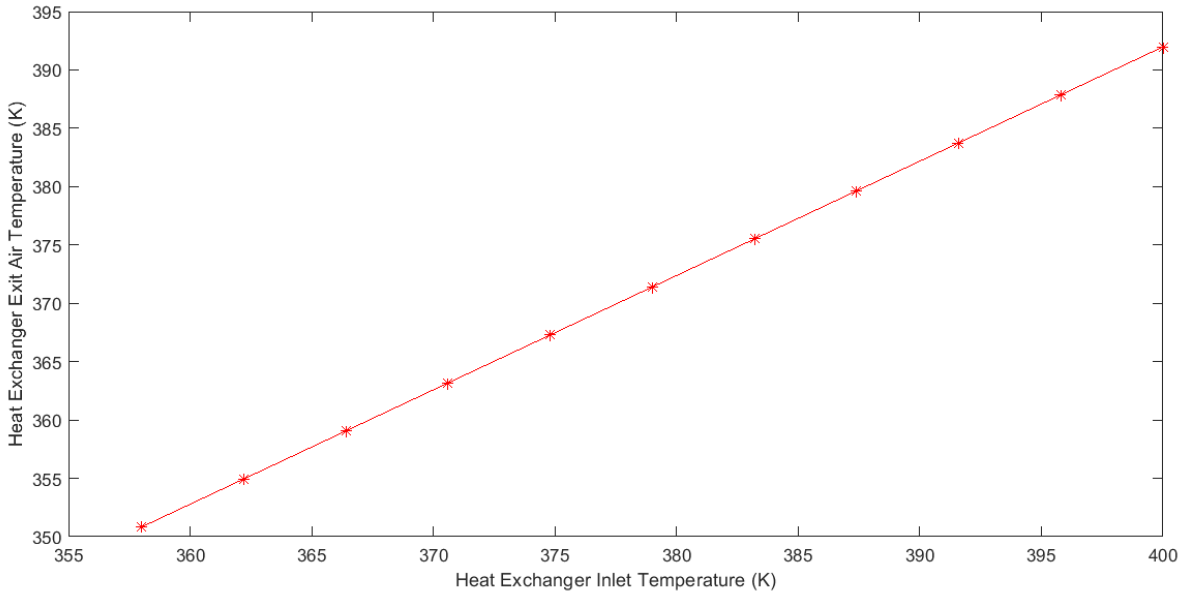

Figure 14:A Graph of Heat Exchanger Heating Fluid Inlet Temperature and the Heat Exchanger Exit Air Temperature

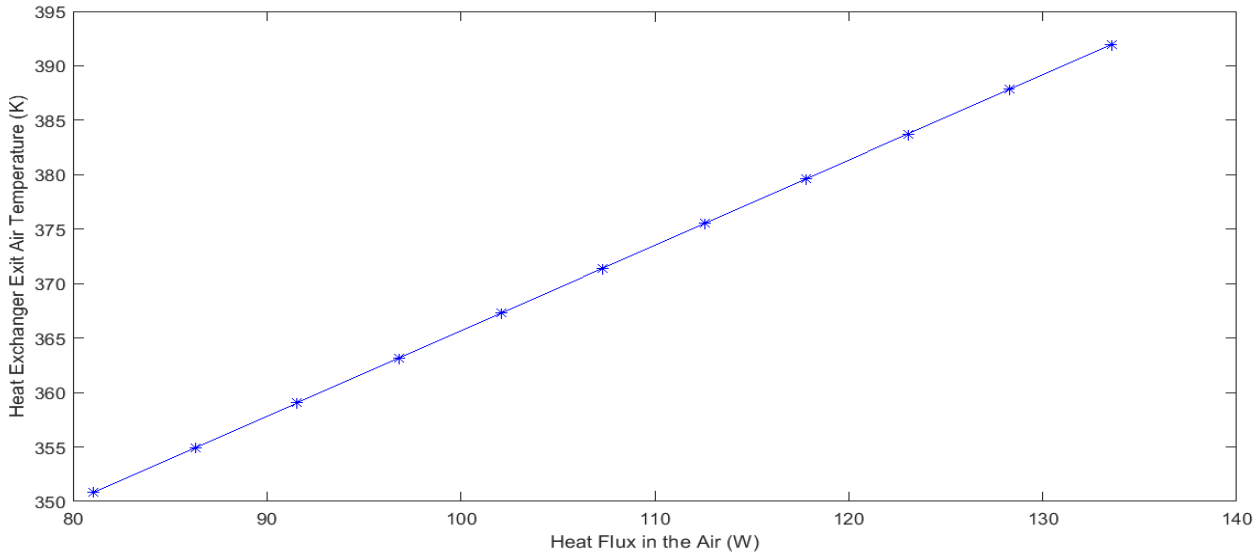

Figure 15: A Graph of Heat Exchanger Exit Air Temperature in relation to the Heat Flux in the Air

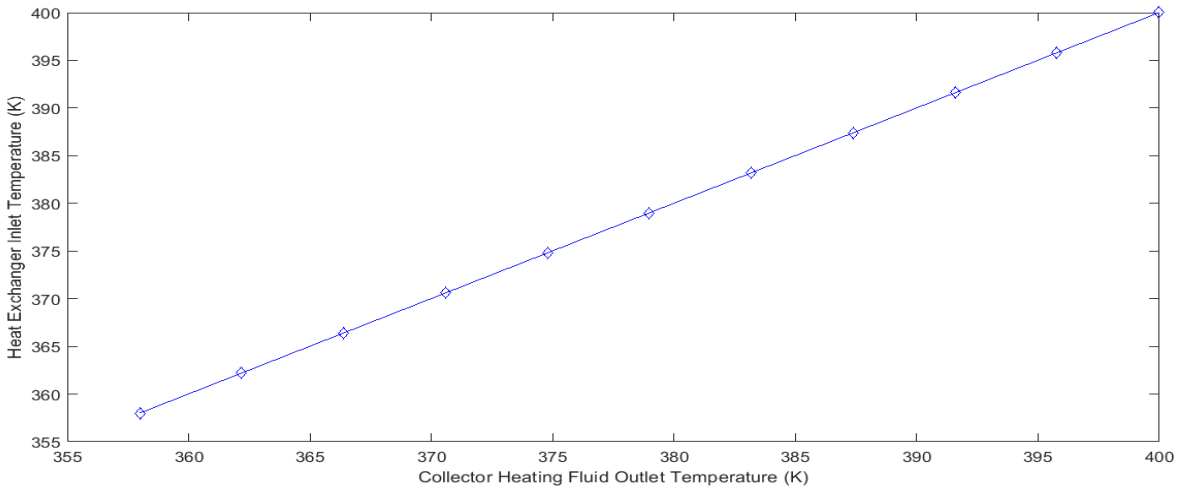

Figure 16: Heat Exchanger Inlet Temperature Plotted against the Collector Heating Fluid Outlet Temperature

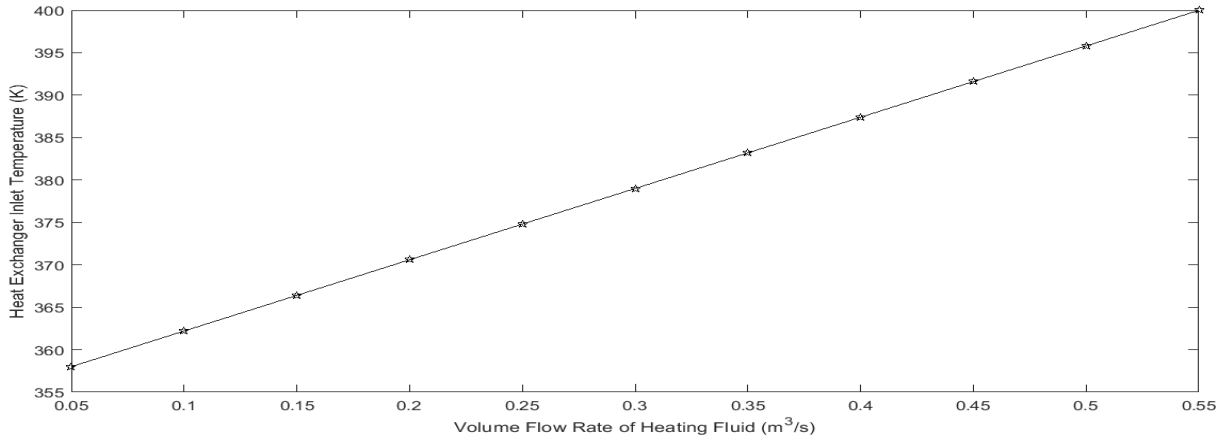

Figure 17: A Plot showing the Influence of Volume Flow Rate of the Heating Fluid on the Heat Exchanger Inlet Temperature

3.1.2 CFD Simulation Results

The Fluent solver was run for 100 iterations for each of the dehydrator configurations. The result of the analysis was obtained through CFD post-processing. This was done using the Ansys Fluent post-processor. Since this study was mainly concerned about the air flow and temperature distribution inside the dehydrator, the variables assessed in the CFD post-processing were relating mainly to air velocity and temperature profile. Results from post-processing the CFD is presented in Figures 18 to 33..

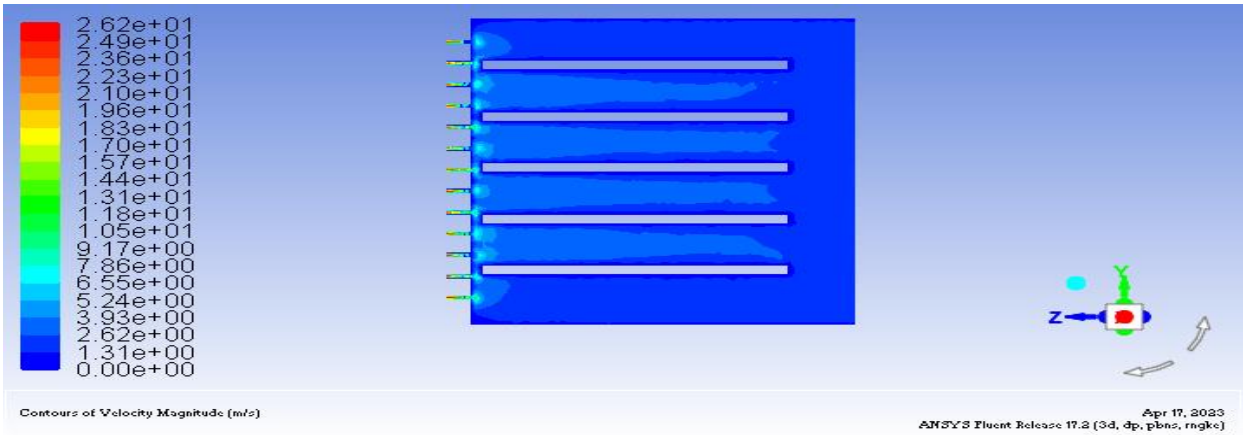

Figure 18: Distribution of Air Velocity Across the Dehydrator with Back Inflow and Front Outflow

Figure 18 shows the simulated airflow across the trays from the back of the dehydrator i.e. right to left. Uniform airflow is noticed across the trays. Flow concentrates at the air outlets. The velocity of air at inlet is 2 m/s; this value is

maintained at different trays with localized increase to 5.24 m/s above the trays. A marked increase is observed at the air exits in front of the dehydrator. At the outlet, the air velocity approaches 15 m/s.

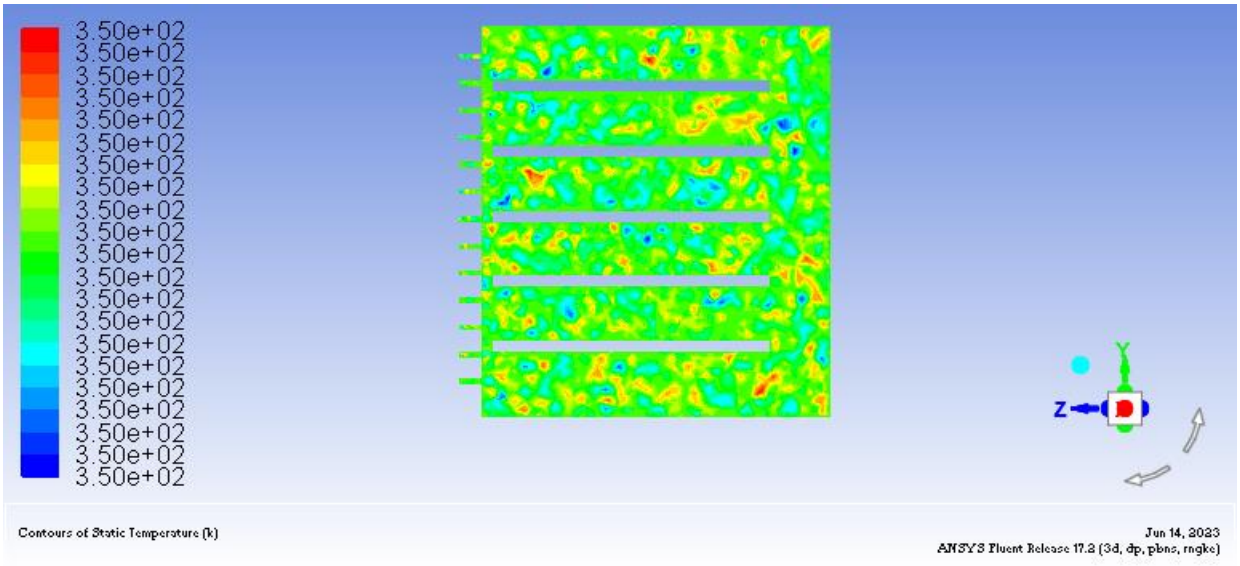

Figure 19: Distribution of Static Temperaturein the Dehydrator with Back Inflow and Front Outflow

The temperature of air at inlet of the drying chamber is 350 K (~77℃). Figure 19 shows that the temperature is distributed across the trays and the entire drying chamber with localized decrease in temperature across the drying chamber.

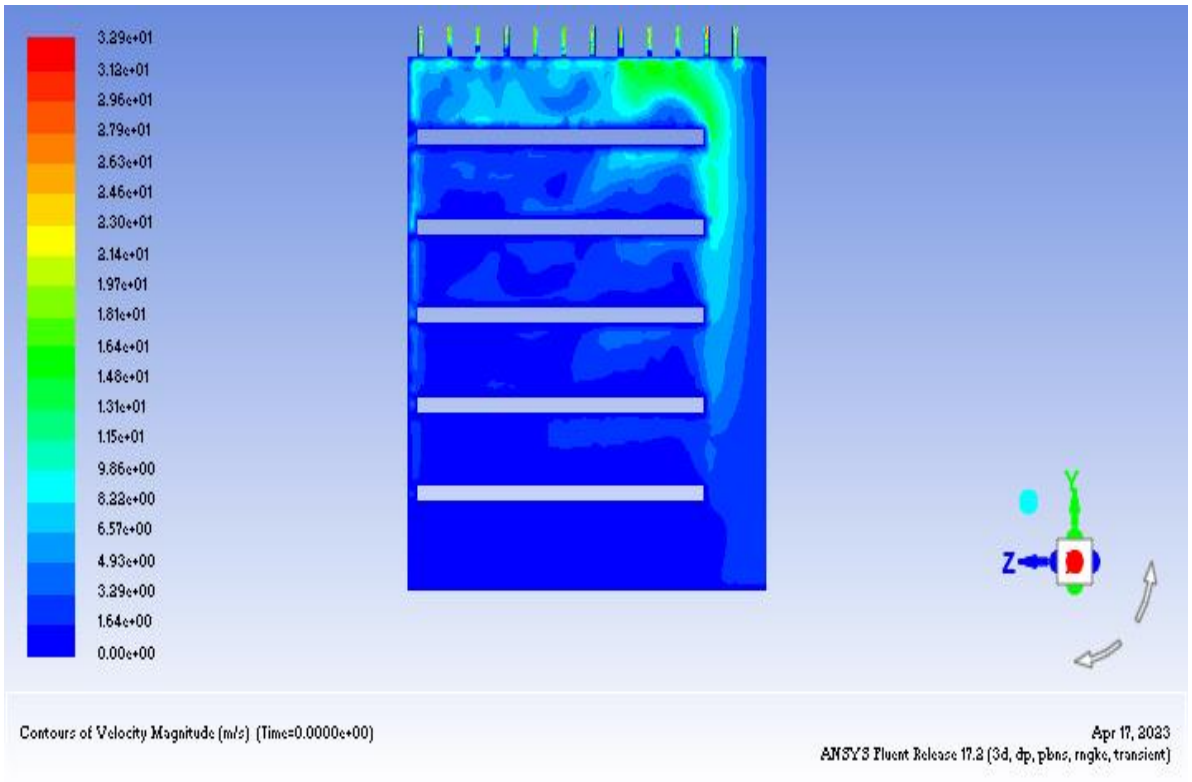

Figure 20: Distribution of Air Velocity across the Dehydrator with Back Inflow and Top Outflow

In Figure 20, the air flows from the back and exits at the top. It can be observed that flow distribution is not uniform. Airflow concentrates at the topmost part of the dehydrator. Thus, the tray closest to the air exits receive more heating air than other trays below it. The inlet velocity of air is 2 m/s, but variations especially in the topmost part of the dehydrator range from 10 to 18 m/s.

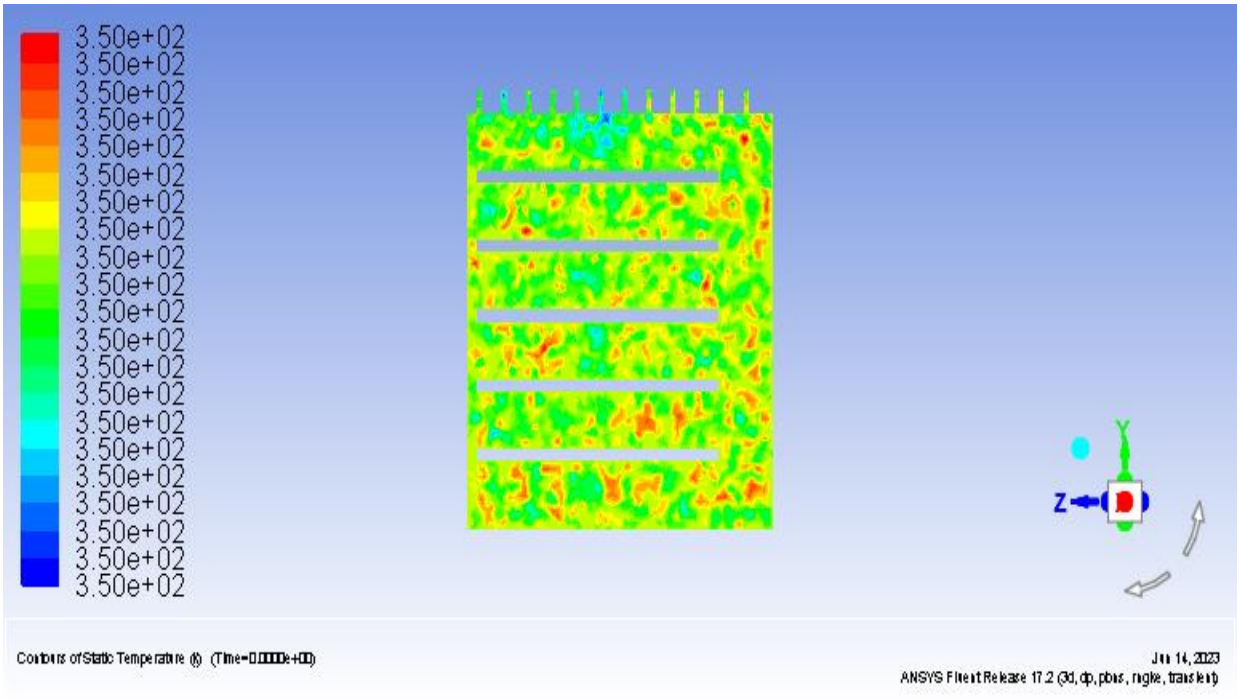

Figure 21: Distribution of Static Temperature in the Dehydrator with Back Inflow and Top Outflow

Figure 21 also shows distribution of static temperature in the dehydrator. The temperature of heat supplied varies throughout the dryer. There are localized reduction in drying air temperature throughout the dryer.

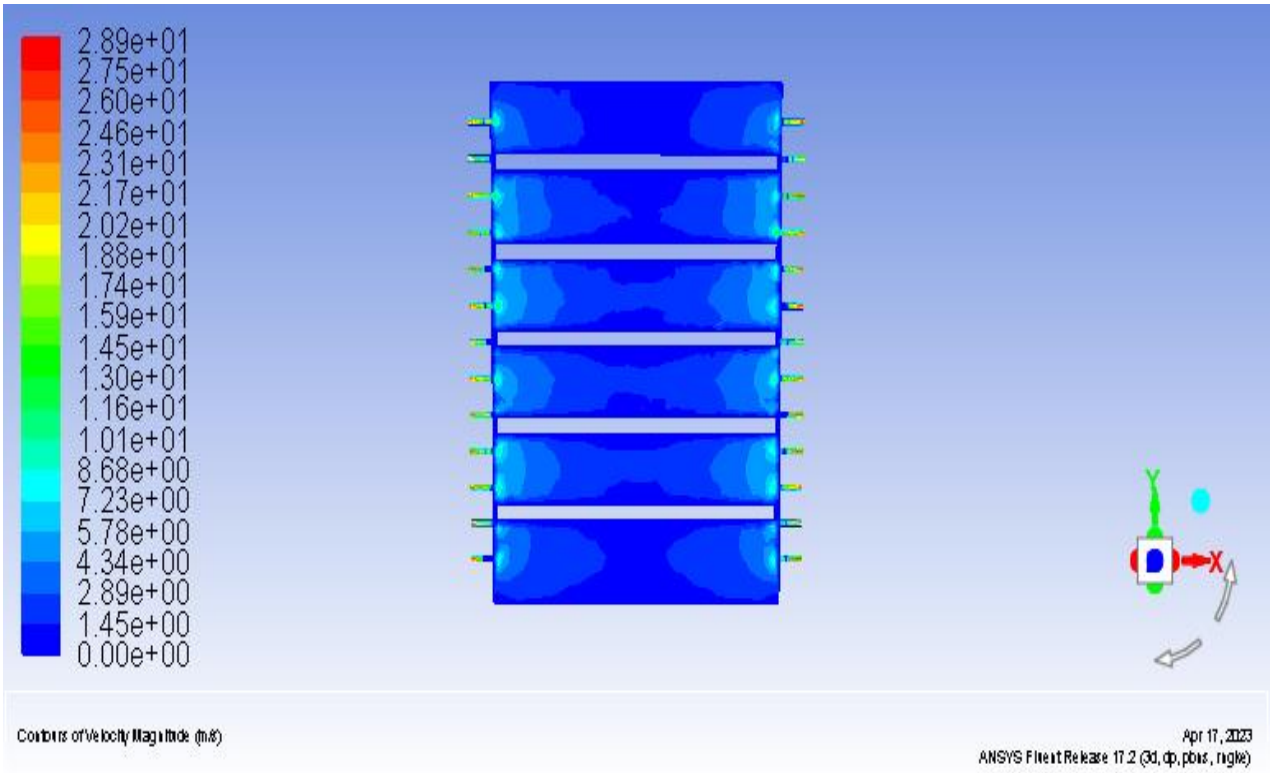

Figure 22: Front View of the Dehydrator Showing the Distribution of Air Velocity with Back Inflow and Side Outflow

In the design shown in Figure 22, air flows into the dehydrator from the back and exits on the sides. It can be observed that flow distribution is fairly uniform across the trays. Flow volume is lesser at the midpoint of the dehydrator and increases to maximum at the exits. Figure 23 shows also that airflow across the trays is uniform as air flows in from the back (right of the page) to side exits towards the door. Figures 23 and 24 also show that the temperature distribution occurs as previously stated in other flow configurations.

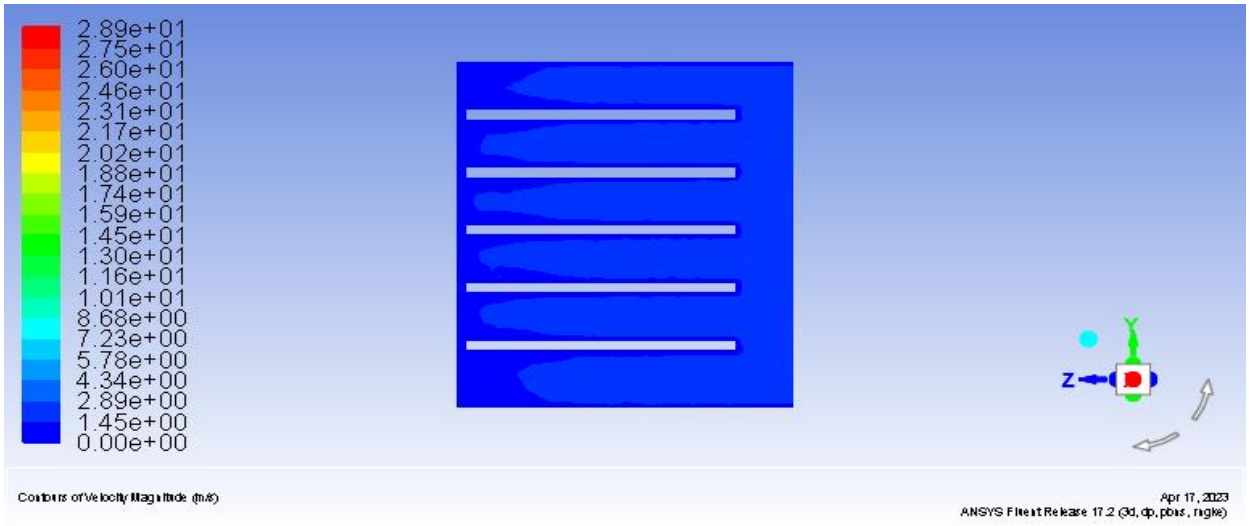

Figure 23:End View of the Dehydrator Showing the Distribution of Air Velocity with Back Inflow and Side Outflow

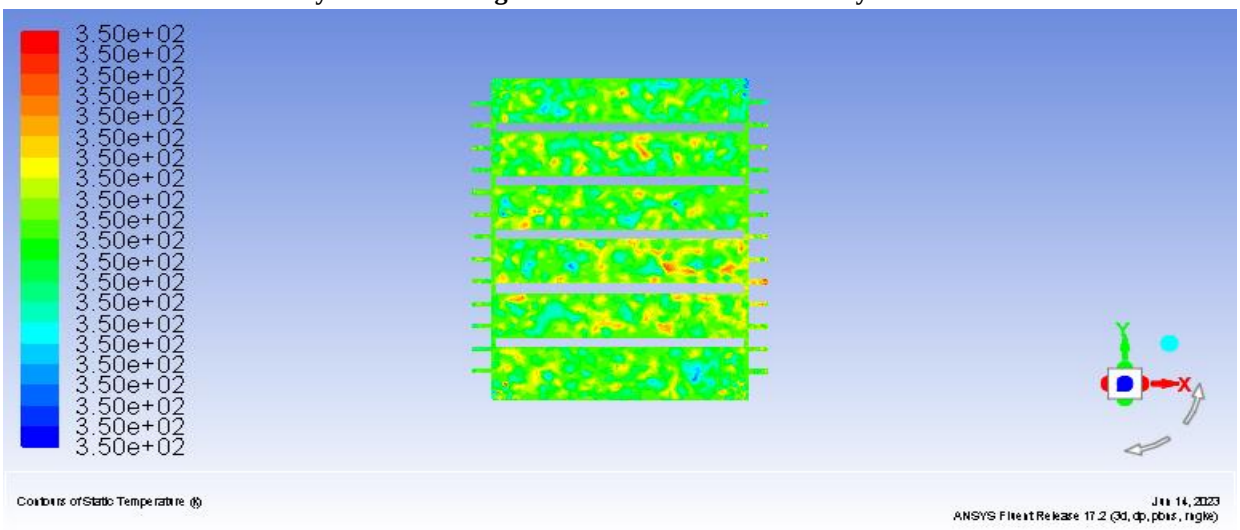

Figure 24:Front View of the Dehydrator Showing the Distribution of Static Temperature with Back Inflow and Side Outflow

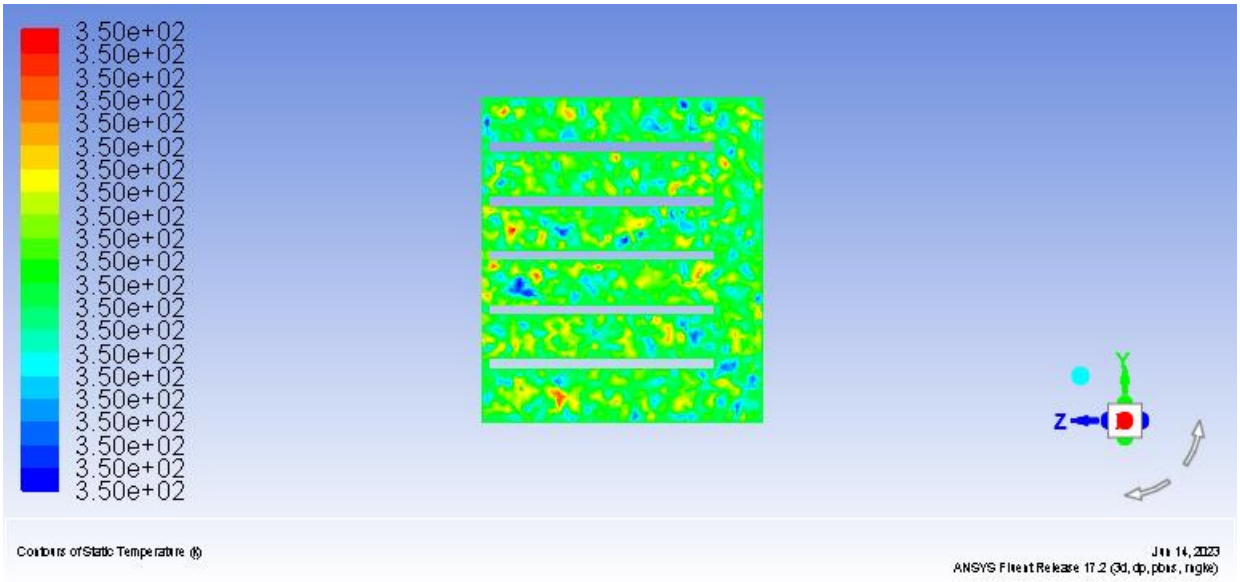

Figure 25: End View of the Dehydrator Showing the Distribution of Static Temperature with Back Inflow and Side Outflow

When air flows in from the bottom (at 2 m/s) and out at the top as shown in Figure 26, more airflow concentrates at the back and moves towards the exit. Although air flows into the tray areas as well, the distribution is non-uniform. Figure 27 shows that the temperature distribution across the trays is not uniform. There are localized decrease from 350 K to 349.5 K.

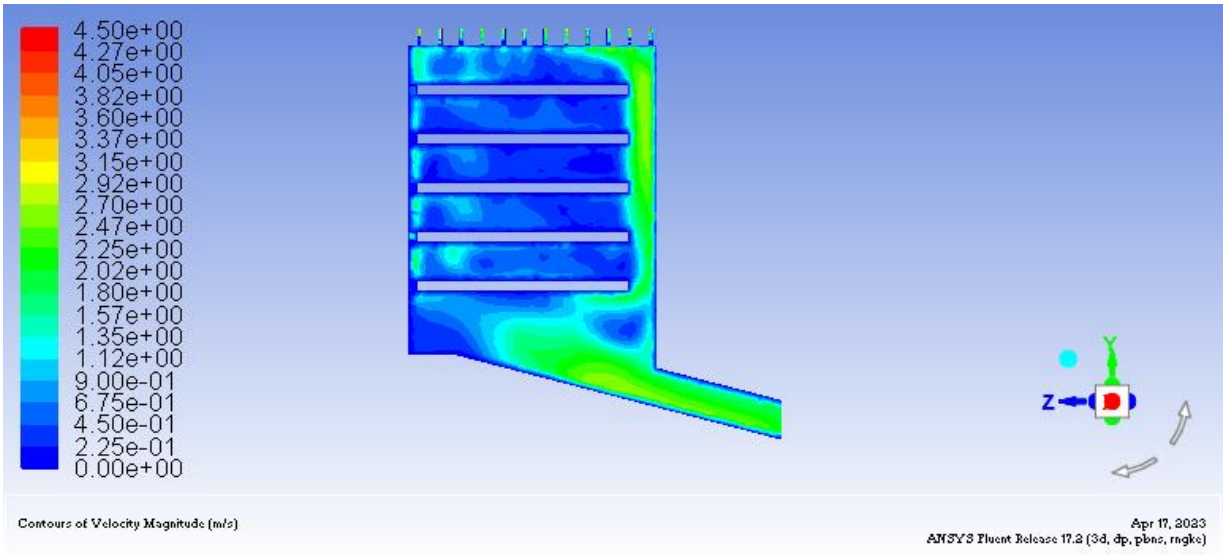

Figure 26: Distribution of Air Velocity Across the Dehydrator with Bottom Inflow and Top Outflow

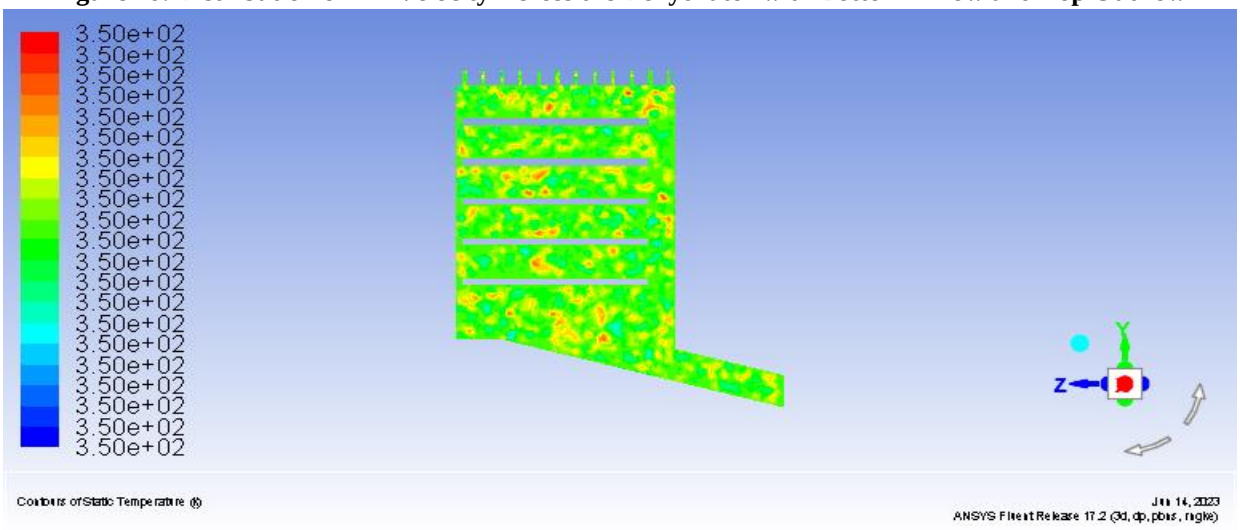

Figure 27: Distribution of Static Temperature Across the Dehydrator with Bottom Inflow and Top Outflow

In Figure 28, it can be observed that air flows from the bottom and exits at the front end of the dehydrator. As a result, more air tends to move upwards at the back of the dehydrator and also toward the air exit at the bottom-most part. Airflow across the trays is non-uniform and temperature varies throughout the dryer as can be seen in Figure 29.

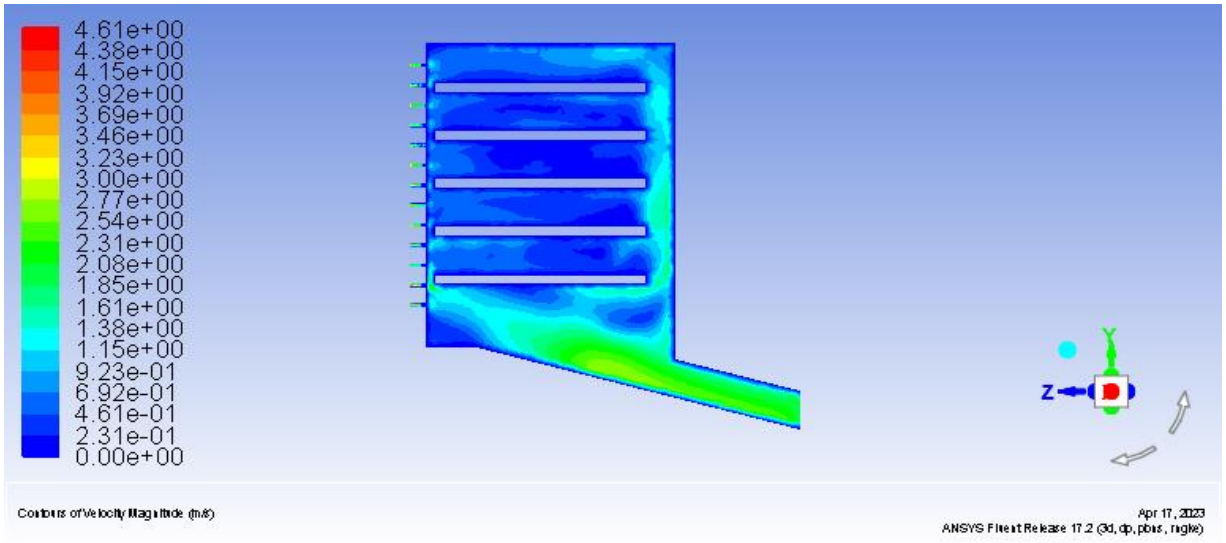

Figure 28: Distribution of Air Velocity Across the Dehydrator with Bottom Inflow and Front Outflow

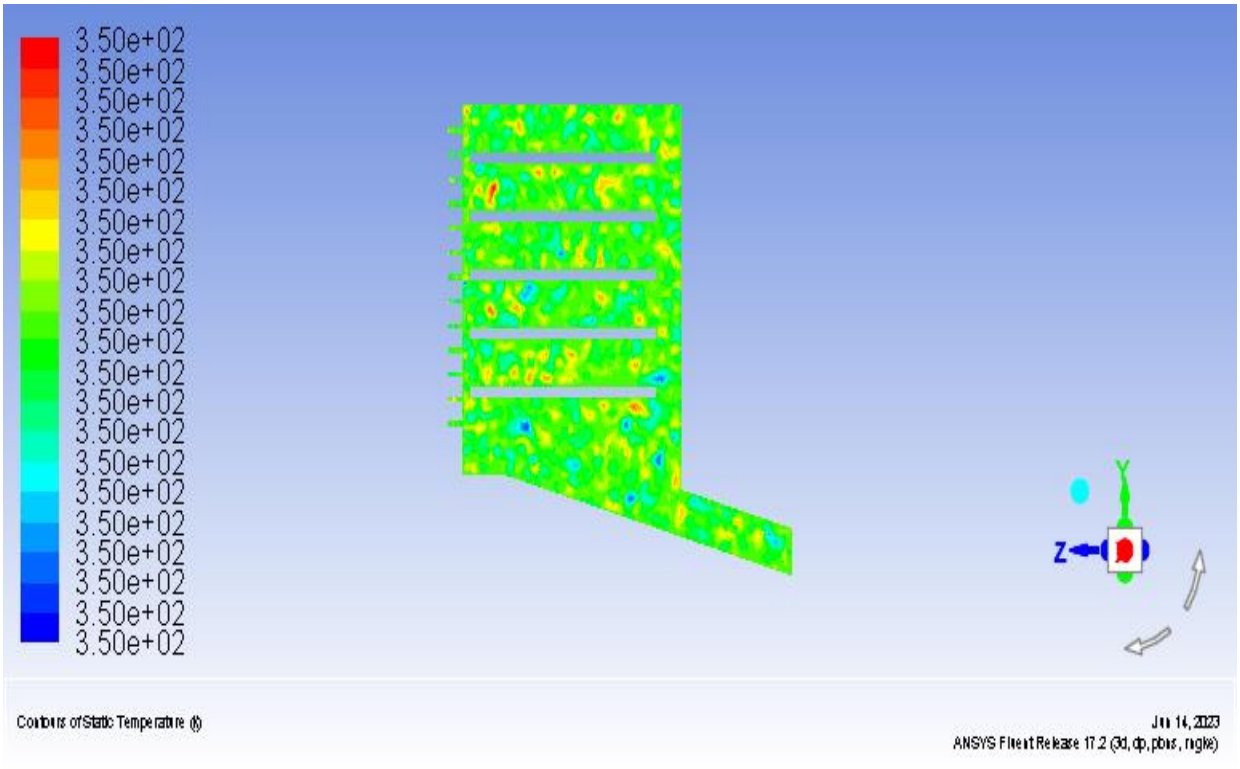

Figure 29: Distribution of Static Temperature Across the Dehydrator with Bottom Inflow and Front Outflow

When air flow is directed from the bottom of the dehydrator through the exit at the sides of the dehydrator, flow distribution seems to be better (Figure 30) compared to other designs where airflow enters the draying chamber from the bottom. When the flow is examined in the end view (Figure 31), it can be observed that the flow distribution does not concentrate so much at the bottom or back of the dehydrator as in the previous designs with bottom in-flow. The temperature distribution across the tray walls vary as shown in Figures 31 to 33.

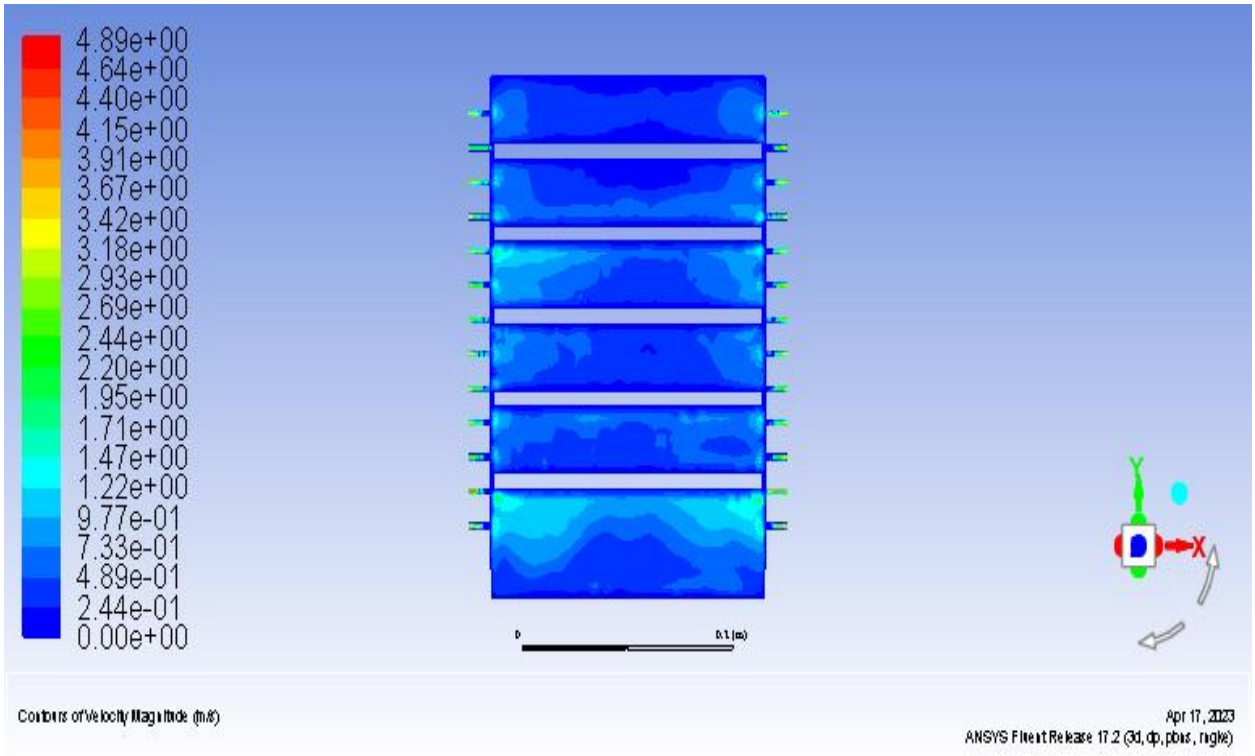

Figure 30:Front View of the Dehydrator Showing the Distribution of Air Velocity with Bottom Inflow and Side Outflow

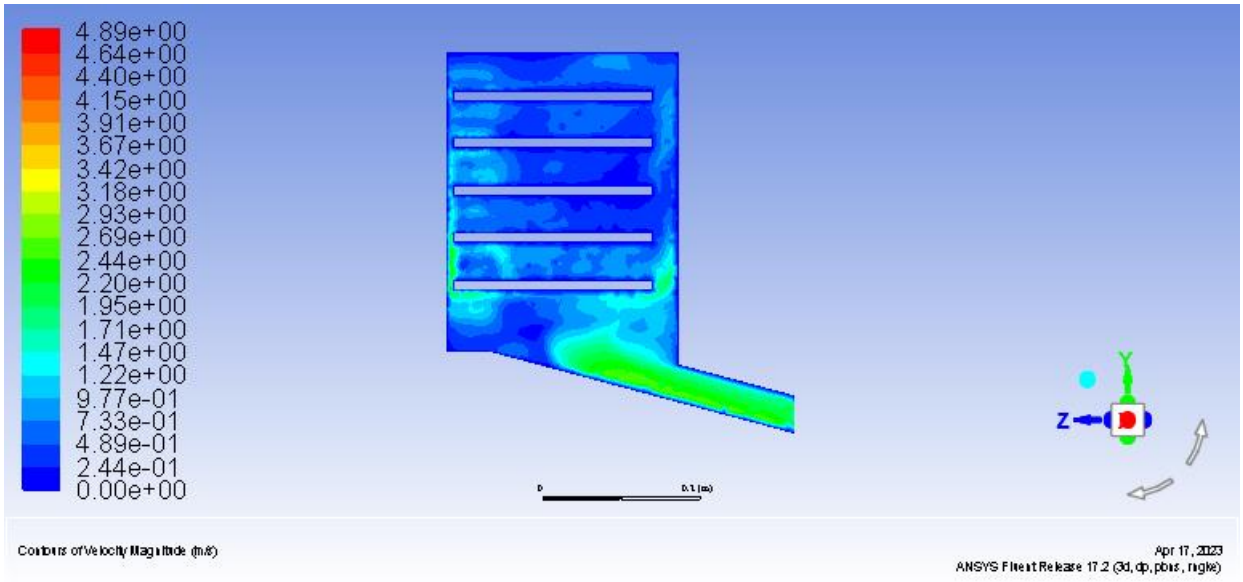

Figure 31:End View of the Dehydrator Showing the Distribution of Air Velocity with Bottom Inflow and Side Outflow

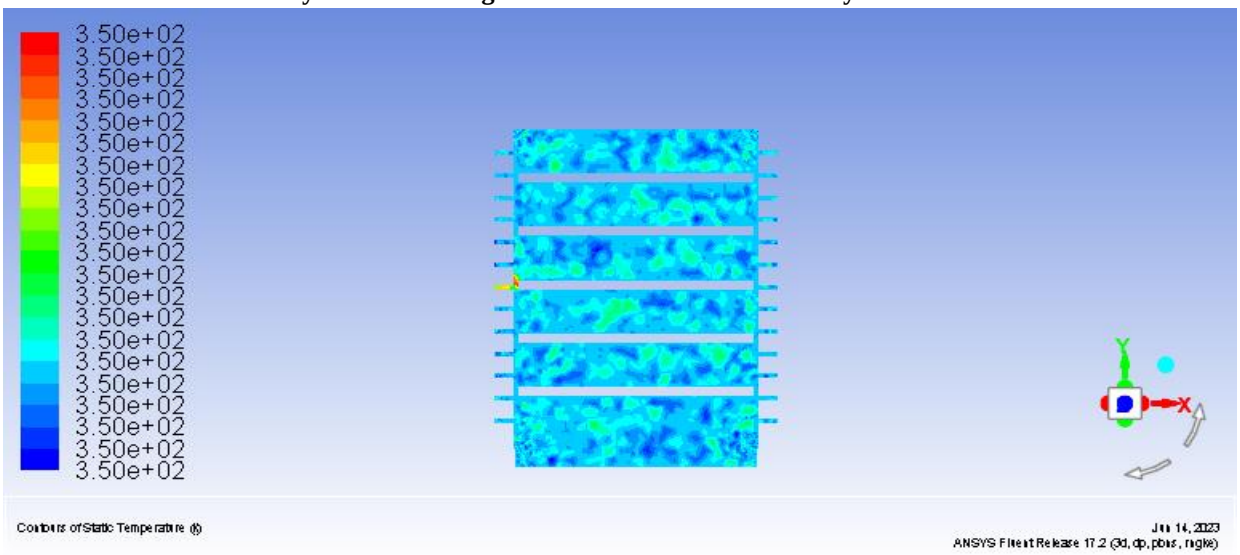

Figure 32:Front View of the Dehydrator Showing the Distribution of Static Temperature with Bottom Inflow and Side Outflow

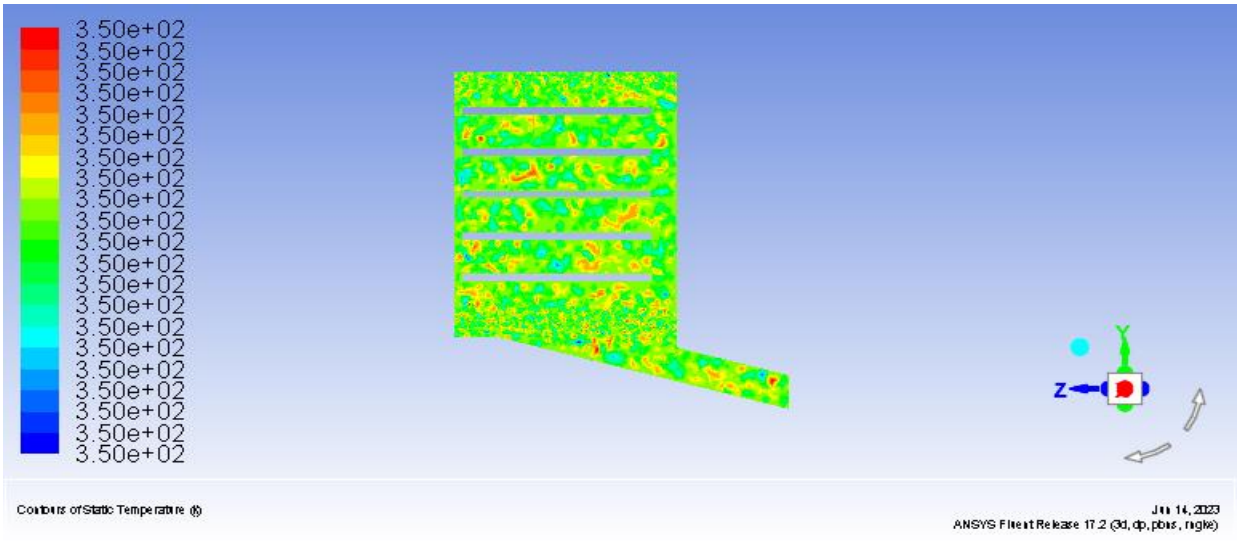

Figure 33:End View of the Dehydrator Showing the Distribution of Static Temperature with Bottom Inflow and Side Outflow

3.2 DISCUSSION

From the data obtained in this study, it is obvious that there is a relationship between the ambient temperature, mass flow rate and the temperature of the heated fluid that exits the solar collector. There is an indication that as the ambient temperature rises, the heated fluid outlet temperature rises, according to the surface plot shown in Figure 13. Also, a higher flow rate is observed to yield lower output temperature of Syltherm 800 at the collector.

In Figure 14, it was observed that the temperature of air leaving the heat exchanger increases in direct proportion to the increase in temperature of Slytherm 800 entering the heat exchanger. This is intuitively adequate, because by the principles of thermodynamics, an increase in heat supplied results in an increase in heat gained by air entering the heat exchanger. This is necessary to ensure thermodynamic equilibrium in the system. In Figure 15, there is an indication also that the heat flux in the heat exchanger has direct impact on the amount of heat transferred to air flowing through the heat exchanger. Heat flux describes the rate at which thermal energy is transferred from one surface to another. In this instance, it is obvious that an increase in the rate of heat transfer from the heating fluid to the surface of the heat exchanger, the higher the temperature of air leaving the heat exchanger.

In Figure 16, there is a comparison between the temperature of heated fluid leaving the PTC and the temperature at the inlet of the heat exchanger. The graph shows direct proportionality in the relationship. Another observation that can be made from the plotted relationship is that only a fraction of heat in the fluid leaving the PTC is lost. The PTC fluid exit temperature is nearly same as the heat exchanger inlet temperature. Furthermore, in Figure 17, it was observed that the volume flow rate of the heating fluid has a direct proportionality to the temperature of fluid at the inlet of the heat exchanger. This occurs because substantial amount of heated fluid carries with it more thermal energy than a lesser amount. When larger quantity of the heated fluid is made to flow through the PTC outlet, the temperature at the inlet of the heat exchanger rises proportionately. These results conform with the findings of [16].

An assessment of the CFD simulation results shown in Figures 18 to 33 indicate that there is variation in the air velocity distribution and temperature in different configurations of the dehydrators. Figure 18 and 19 show that the back inflow - front outflow configuration provides uniform distribution of heated air in the drying chamber. There is very small variation observed on each tray compared to other configurations. This uniformity is also observed in the distribution of static temperature for this configuration. Similar performance in flow and temperature distribution is observed in Figures 22, 23, 24 and 25 in the back inflow – side outflow configuration. These results are consistent with the observations of [21]. Supply of airflow across the trays horizontally provides best temperature and airflow distribution.

The flow distribution in the back inflow – top outflow shows a substantial increase in air velocity at the upper trays than the lower trays. The highest amount of flow rise was observed at the topmost tray – close to the air exit with velocities approaching 20 m/s. In Figure 21, the static temperature distribution shows also that the trays closest to the top have higher temperature at the region closest to the dehydrator door i.e. opposite the region with highest velocity distribution. The temperature distribution around the trays show uniform distribution of heat across the trays with localized reductions in temperature from 350 K to 349 K.

Figure 26 shows that in the bottom inflow – top outflow configuration, there is uneven velocity distribution inside the drying chamber. Air velocity at the back of the dehydrator is high, with uneven velocity distribution noticed in areas around the tray. The static temperature profile (Figure 27) indicates temperature variations across the dehydrator. Similar result is obtained in the bottom inflow – front outflow configuration; although the variation of flow above the trays tend to be lesser than in the bottom inflow – top outflow configuration. Also, the static temperature in the bottom inflow – front outflow configuration is more uniform than in the bottom inflow - top outflow configuration. This result is consistent with the observations of [9].

Furthermore, the velocity and temperature distribution in the bottom inflow – side outflow configuration shown in Figures 30, 31 and 32 indicate non-uniformity. Comparatively, the result in this configuration is better than that of the top outflow configuration.

4.0 CONCLUSION

Supply of airflow across the trays horizontally provides best airflow and temperature distribution in solar dehydrators. The research found that an increase in the heat supplied results in an increase in heat gained by air entering the heat exchanger, necessary to ensure thermodynamic equilibrium in the system. The heat flux in the heat exchanger has a direct impact on the amount of heat transferred to air flowing through the heat exchanger. The volume flow rate of the heating fluid has a direct proportionality to the temperature of fluid at the inlet of the heat exchanger.

The CFD simulation results showed that the back inflow - front outflow configuration provides uniform distribution of heated air in the drying chamber, while the bottom inflow – top outflow configuration showed non-uniformity. The simulations were carried out with inlet conditions of 2 m/s in air velocity and 350 K in temperature. The study suggests that the optimization of a solar dehydrator design should consider the distribution of temperature and airflow in the drying chamber to ensure quality dried foods. These results were found to conform with similar previous studies on the same subject. This research can be further developed to model and

optimize other parameters such as the relative humidity, thickness of the fruit to be dried and tray spacing

REFERENCES

1. Fuchs, H. (2010). The Dynamics of Heat: A Unified Approach to Thermodynamics and Heat Transfer. Springer Science + Business Media, New York, 99-150.
2. Roustapour, O., Gazor, H. and Farzin, K. (2019). Numerical Modelling of Air Flow in a Cabinet Dryer Equipped by Deflector Plates. *International Journal of Food Engineering.* DOI: 10.1515/Ijfe-2018-0341.
3. Jangam, S., Law, C. and Mujumdar, A. (2010). Drying of Foods, Vegetables and Fruits. National University of Singapore, Singapore, 2-10.
4. Gangloff, T, Gangloff, S., and Ferguson, S. (2014). The Ultimate Dehydrator Cookbook, Stackpole Books, Mechaniscsburg, 17 – 120.
5. Hall, W. and Keynes, M. (2016). Introduction to Finite Element Analysis. The Open University. Retrieved on 3rd August 2021. Available at: www.open.edu/openlearn/science-maths-technology/introduction-finite-element-analysis/content-section0?utm_source=openlearnutm_campaign=olutm_medium=ebook
6. ANSYS (2006). Introduction to CFD Analysis: Introductory FLUENT Training. Retrieved on 3rdAugust 2021. Available at: www.slideshare.net/waseemayesh2/1-intro-to-cfd-analysis
7. Dinçer, I. and Rosen, M. (2011). Thermal Energy Storage Systems and Applications. John Wiley and Sons Ltd., West Sussex, 83 – 90.
8. Mitchell, E. (2021). Dehydrator Air Flow: Horizontal or Vertical? Retrieved on 3rd August 2021. Available at: dehydratorlab.com/vertical-air-flow-vs-horizontal-air-flow
9. Getahun, E, Delele, M., Gabbiye, N., Fanta, S., Demissie, P. and Vanierschot, M. (2021). Importance of Integrated CFD and Product Quality Modelling of Solar Dryers for Fruits and Vegetables: A Review, *Elsevier*, 220: 88-110.
10. Vanek, F and Albright, L. (2008). Energy Systems Engineering: Evaluation and Implementation. McGraw Hill, New York, 168 – 295.
11. Motahayyer, M., Arabhosseini, A. and Samimi-Akhijahani, H. (2019). Numerical Analysis of Thermal Performance of a Solar Dryer and Validated with Experimental and Thermo-graphical Data. Elsevier, 193: 692-705.
12. Kalogirou, S. (2009). Solar Energy Engineering: Processes and Systems. Elsevier Inc., California, 140 - 250.
13. Getahun, E, Gabbiye, N.,Delele, M., Fanta, S. Gebreslasie, M., and Vanierschot, M. (2020 Effect of Maturity on the Moisture Sorption Isotherm of Chilli Pepper (MarekoFana Variety).Heliyon. https://doi.org/10.1016/j.heliyon.2020.e04608.
14. Sulaksna, K. and Thamatkeng, P. (2014). Heat Transfer and Fluid Flow Simulation withANSYS. Retrieved on 3rd August2021. Available at: eng.sut.ac.th/me/2014/document/training/CAETraining(Fluid).pdf&ved=2ahUKEwib8Mmo8PL1AhWR3oUKHQdwDp0QFnoECDAQAQ&usg=AOvVaw2zWi-ilAAjWcNg7qNHpe8f
15. Chen X. and Liu, Y. (2015). Finite Element Modelling and Simulation with ANSYS Workbench, Taylor and Francis Group, New York, 1-50.
16. Bellos, E and Tzivanidis, C. (2018). Analytical Expression of Parabolic Trough Solar Collector Performance. *Designs*. 2(9): 1 – 17. doi:10.3390/designs2010009.
17. DOW (1997). Sylltherm 800 Heat Transfer Fluid: Product Technical Data. DOW Chemical Company, Canada, 15.
18. Duffie, J. and Beckman, W. (2013). Solar Engineering of Thermal Processes. John Wiley and Sons, New Jersey, 168 – 170.
19. Incropera, F., Dewitt, D., Bergman, T., and Lavine, A. (2017). Fundamentals of Heat and Mass Transfer (8th ed.). John Wiley and Sons, 359 – 362.
20. Cadence CFD (2023). FEA vs. CFD: The Differences and Applications of Simulation Tools. Accessed on 20th February, 2023. Available at:https://resources.systemanalysis.cadence.com/blog/msa2021-fea-vs-cfd-the-differences-and-applications-of-simulation-tools
21. Sileshi, S., Hassen, A., and Adem, K. (2022). Simulation of Mixed-Mode Solar Dryer with vertical Air Distribution Channel. Elsevier Ltd. 1-11. https://doi.org/10.1016/j.heliyon.2022.e11898.